The wake of two side-by-side square cylinders

MD MAHBUB ALAM[1,2], Y. ZHOU[1]†, AND X. W. WANG[1,3]

[1]Department of Mechanical Engineering, The Hong Kong Polytechnic University, Hung Hom, Kowloon, Hong Kong

[2]Department of Mechanical and Aeronautical Engineering, University of Pretoria, Pretoria 0002, South Africa

[3]Key Laboratory of Manufacture and Test Techniques for Automobile Parts, Chongqing University of Technology, China

Aerodynamic interference between two cylinders involves most of the generic flow features associated with multiple structures, thus providing an excellent model for gaining physical insight into the wake of multiple cylindrical structures. This work aims to provide an experimental systematic study of the flow behind two side-by-side square cylinders. The square cylinder is a representative model for bluff bodies with sharp corners, characterized by a fixed flow separation point, which are distinct from those of continuous curvature with oscillating separation points, typically represented by the circular cylinder. Experiments were performed at a Reynolds number Re of 4.7×10^4 and a cylinder centre-to-centre spacing ratio T/d (d is the cylinder height) of 1.02–6.00. The flow was measured using different techniques, including hot wires, load cell, particle imaging velocimetry and laser-induced fluorescence flow visualization. Four distinct flow regimes and their corresponding T/d ranges are identified for the first time on the basis of the flow structure and the Strouhal number. Physical aspects in each regime, such as interference between shear layers, gap flow deflection and changeover, multiple flow modes, entrainment, recirculation bubble, vortex interactions and formation lengths, are investigated in detail and are connected to the characteristics of the time-averaged and fluctuating fluid forces. The flow displays a marked difference in many facets from that behind two side-by-side circular cylinders, which is linked to their distinct flow separation natures. A crucial role played by the gap flow and its passage geometry in contributing to the observed difference is also unveiled.

Key words: flow–structure interactions, separated flows, vortex streets

1. Introduction

Slender engineering structures are frequently seen in groups, for example high-rise buildings, chimney stacks, tube bundles in heat exchangers, overhead power-line bundles, bridge piers, stays, masts, chemical-reaction towers and offshore platforms. Naturally, it is important to understand the proximity effect on aerodynamics associated with multiple closely separated cylindrical structures. The simplest configuration of multiple structures is two cylindrical structures in tandem, side-by-side or staggered arrangements. The flow around two cylindrical structures

† Email address for correspondence: mmyzhou@inet.polyu.edu.hk

involves most of the generic flow features (flow separation, interference between shear layers, quasi-periodic vortices, vortex impingement, gap flow instability, recirculation, interacting streets, distinct flow modes, etc.) associated with multiple structures, thus providing an excellent model for gaining insight into flow physics of more structures.

Aerodynamically, the cylindrical structures may be divided into three categories: (i) cross-sectional shapes with continuous and finite curvature (e.g. circular and elliptical cylinders), where flow separation may oscillate and occur over a segment of the surface, depending on the surface condition, the Reynolds number Re, etc.; (ii) cross-sectional shapes with sharp corners of an infinitely large curvature (e.g. flat plates and square and triangular cylinders), where the flow separation point is fixed; (iii) a combination of (i) and (ii), such as the D-shaped cylinder and square cylinders with rounded corners. For category (i), the flow is highly dependent on the initial flow conditions (Re, turbulent intensity, surface roughness, etc.) because of the non-stationary oscillation nature of the flow separation point. For category (ii), however, the Re effect is insignificant because flow separation is fixed at the sharp corners. Circular and square cylinders are generally chosen as the representative models of categories (i) and (ii), respectively, because of their relative simplicity and also because of their most frequent occurrence in engineering.

There have been extensive investigations on the wake of two side-by-side circular cylinders. Three flow regimes have been identified (Ishigai *et al.* 1972; Zdravkovich 1977). The 'single-bluff-body regime' occurs at the cylinder centre-to-centre spacing ratio $T/d < 1.2$–1.3, where the two cylinders behave like one structure, generating a single vortex street with one predominant Strouhal number St (Spivack 1946). The d the cylinder diameter for circular cylinder or the height for square cylinder (figure 1). The 'asymmetrical wake regime' occurs at T/d values between 1.2–1.3 and 2.2–2.5, where the gap flow between the cylinders is biased, resulting in one wide and one narrow street (figure 1), and one low and one high St, respectively (e.g. Bearman & Wadcock 1973). The gap flow in this regime switches spontaneously from one side to the other; thus this regime is often referred to as the 'bistable' or 'flip-flopping' regime (Kim & Durbin 1988; Moreti 1993). At $T/d > 2.2$–2.5, two coupled vortex streets (CVS) of the same St are generated, which are either in-phased or anti-phased and are frequently called the 'coupled-street regime' (e.g. Kamemoto 1976; Meneghini *et al.* 2001). The two in- and anti-phased streets correspond to a phase shift of 0° and 180°, respectively, between vortex sheddings from the two cylinders (e.g. Thomas & Kraus 1964). The critical T/d that divides the regimes depends on Re (Xu, Zhou & So 2003).

Much attention has been given to the time-averaged forces on two side-by-side circular cylinders in different regimes. Biermann & Herrnstein (1933) measured the time-averaged drag force coefficient (C_D) at $Re = 6.5 \times 10^4$. The maximum C_D was found at $T/d = 1.05$ in the single-bluff-body regime and the minimum at $T/d = 1.3$ in the asymmetrical flow regime, about 60% higher and 46% lower, respectively, than its counterpart (C_{D0}) in a single isolated cylinder. It was further noted that C_D in the CVS regime was slightly higher at $T/d = 2$–5 than C_{D0} but dropped to the same value for $T/d > 5$. However, they did not attempt to measure C_D separately for the narrow- and wide-street modes, since the gap flow switches randomly in the asymmetrical regime. Zdravkovich & Pridden (1977) measured C_D and the time-averaged lift force coefficient (C_L) at $Re = 6 \times 10^4$ for the narrow- and wide-street modes, respectively. In order to make the two modes sufficiently stable, they made the cylinders slightly staggered. A high and a low C_D ($T/d = 1.2$–2.2) were found to correspond to the narrow and wide streets, respectively, and their sum was always less than $2C_{D0}$, as the measurements of Hori (1959) at $T/d = 1.2$ and 3.0 ($Re = 8 \times 10^3$)
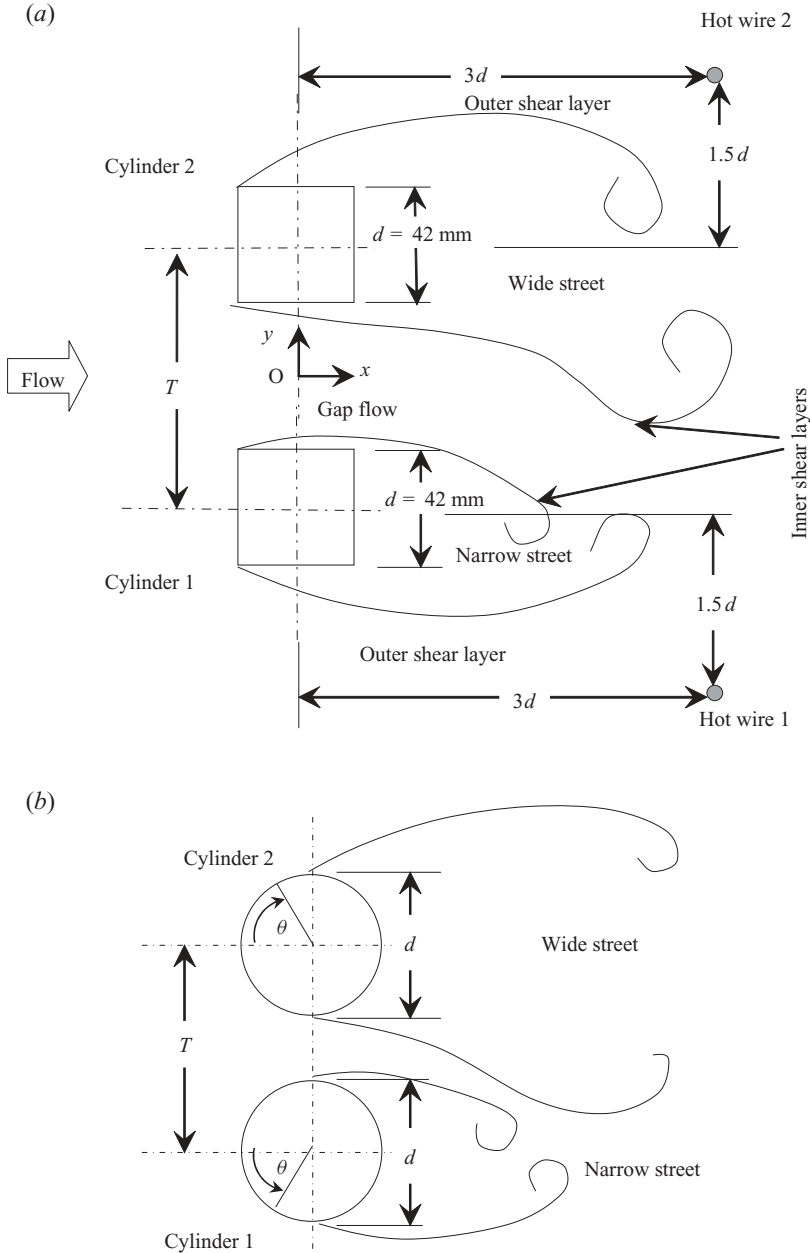
FIGURE 1. (*a*) Schematic of square cylinders and hot-wire arrangement and the definition of the coordinate system. (*b*) The definitions of symbols for two side-by-side-arranged circular cylinders.

indicated. A similar observation was made by Zhou *et al.* (2001) at $T/d = 3.0$ and $Re = 3.5$–10.4×10^3. However, Alam, Moriya & Sakamoto (2003*a*) observed that this sum was higher at $T/d < 1.15$ and 2.1–5.0 and only lower for $T/d = 1.15$–2.1 than $2C_{D0}$. Previous investigators (Hori 1959; Bearman & Wadcock 1973; Zdravkovich & Pridden 1977; Jendrzejczyk & Chen 1982; Zhou *et al.* 2001) noted that C_L on two side-by-side cylinders was always repulsive and decreased with increasing T/d.

Alam, Sakamoto & Moriya (2003b) measured attractive C_L at very small T/d, i.e. $T/d = 1.1$, where the gap flow swept around one cylinder for a longer peripheral length, forming a separation bubble (see also Alam & Zhou 2007a). In contrast to the numerous studies of C_D and C_L, there have been very few studies of unsteady fluid forces on two cylinders. Alam *et al.* (2003a) measured C_D, C_L, root-mean-square (r.m.s.) lift and drag coefficients (C_L', C_D') and St at $T/d = 1.1$–6.0 and $Re = 5.5 \times 10^4$. The narrow street was found to be associated with higher C_L' and C_D' than the wide street. Furthermore, C_L' and C_D' were significantly higher at $T/d = 2.0$–4.0 than at $T/d = \infty$ (single or non-interacting cylinder), with their maximum occurring at $T/d = 2.2$, exceeding their counterpart in a single-cylinder wake by 46 % and 50 %, respectively.

In spite of its great relevance to engineering, the flow around two square cylinders has received much less attention than the wake of two circular cylinders. There have been scattered investigations on the wake of two side-by-side square cylinders. Sakamoto & Haniu (1988) investigated aerodynamic forces, St and cross-correlation between fluctuating pressures on two side-by-side square prisms, with an aspect ratio of 3, immersed in a thick turbulent boundary layer. No end plates were mounted; T/d examined was between 1.2 and 7.0, and Re based on the characteristic width of the prism was 1.52×10^5. They failed to observe the bistable phenomenon of the flow. Using a two-component laser Doppler velocimetry, Kolář, Lyn & Rodi (1997) measured the wake of two side-by-side square cylinders ($Re = 2.3 \times 10^4$) at $x/d = 1$–9, where x was the streamwise distance from the cylinder centres. They examined the flow only at $T/d = 3$, where two coupled vortex streets occurred, providing no information on the flow in other possible regimes. Agrawal, Djenidi & Antonia (2006) investigated numerically the laminar wake ($Re = 73$) of two side-by-side square cylinders at $T/d = 1.7$ and 3, using a lattice Boltzman method. They observed both in- and anti-phased vortex sheddings from the two cylinders at $T/d = 3$ and a biased gap flow at $T/d = 1.7$, which could switch randomly from one side to the other, forming a narrow and a wide street behind the cylinders. The observation is similar to that behind two side-by-side circular cylinders. Also using a lattice Boltzmann method, Rao, Ni & Liu (2008) examined the flow structure, C_D and St at $T/d = 2.0$–3.7 ($Re = 73$–200). The gap flow between the cylinders was biased at $T/d < 2.5$, forming a narrow and a wide street. The narrow street corresponded to a higher C_D and St than the wide street. At $T/d > 2.5$ two coupled streets, either in-phased or anti-phased, were observed.

None of the above investigations attempted to provide a systematic study of this flow. Naturally, many important issues have yet to be addressed. For instance, as is well known, the flow separation point oscillates in a non-stationary fashion on a circular cylinder but is fixed on a square cylinder; the ensuing aerodynamic interferences between two cylinders should be rather different between the two cases. Other questions also follow. How would this difference affect the near-wake characteristics? Would it have a pronounced impact upon the classification of flow regimes? The fluid forces on two side-by-side square cylinders cannot be the same as on two circular cylinders, as may be inferred from distinct surface pressure distributions around the two types of cylinders (e.g. Vickery 1966; Achenbach 1968; Batham 1973; Bearman & Obajasu 1982; West & Apelt 1993; Alam *et al.* 2002, 2003b; Alam & Sakamoto 2005; Alam, Sakamoto & Zhou 2005). Then, how do steady and unsteady fluid forces and St vary with T/d, in particular in the turbulent subcritical flow regime?

In order to address the issues raised above, this work sets out to measure systematically the flow structure, St and fluid forces (C_D, C_L, C_D', C_L') and their
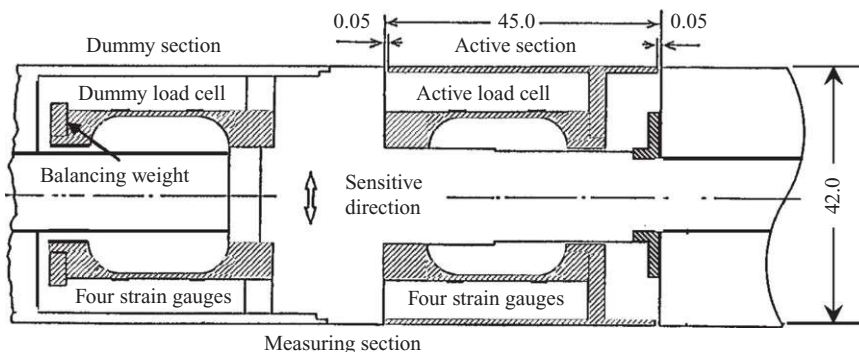
FIGURE 2. Installation of load cells inside a square cylinder. The measurements
are in millimetres.

dependence on T/d in the turbulent wake of two side-by-side square cylinders, with
a view to provide a relatively thorough understanding of this flow, including its
classification of different regimes. The T/d range examined is from 1.02 to 6.00,
covering all possible flow regimes; C_D, C_L, C'_D and C'_L are measured using a load cell,
and St is obtained from hot-wire-measured fluctuating streamwise velocity of the flow.
The flow structure, including the non-stationary gap flow switch in the intermediate
range of T/d, is carefully examined on the basis of particle imaging velocimetry (PIV)
and laser-induced fluorescence (LIF) flow visualization measurements. The correlation
between the fluid dynamic forces and the characteristic parameters of the wake is
also discussed.

2. Experimental details

2.1. *Force and St measurements*

Fluid force measurements were conducted in a closed-circuit wind tunnel with a
test section of length 2.2 m, width 0.3 m and height 1.2 m in the Fluid Mechanics
Laboratory of the Kitami Institute of Technology, Japan. Two square cylinders of a
width $d = 42$ mm, made of brass, spanned horizontally across the test-section width.
The free-stream velocity U_∞ was 17 m s^{-1}, resulting in Re ($\equiv U_\infty d/\nu$) $= 4.7 \times 10^4$, where
ν is kinematic viscosity of air. The flow non-uniformity was within ± 0.2 % (r.m.s.)
within the central cross-sectional area of 0.24 m $\times$ 0.95 m in the test section, and the
longitudinal turbulence intensity was less than 0.5 % in the absence of the cylinders.
More details of the tunnel are given in Alam *et al.* (2005). A schematic diagram of
the cylinder arrangement is given in figure 1, along with the definitions of symbols.
The Cartesian coordinate system was defined such that the origin was at the midpoint
between the two cylinders, with the x-axis and the y-axis along the streamwise and
lateral directions, respectively.

Fluid forces were measured over a small spanwise length of the cylinders, using
load cells. The cylinder to be measured was built in with an active ('live') section of
a spanwise $1.07d$ length and two dummy sections. The active section, placed between
the two dummy sections, corresponded to the midspan of the cylinder and was
installed with a load cell that consisted of four semiconductor strain gauges (figure 2).
One of the dummy sections was also instrumented with another load cell of the
same configuration. The load cell inside the active section measured a combination of
fluid forces and forces due to vibration transmitted from outside through the cylinder
support, whilst that inside the dummy section measured the latter forces only. Hence,

the fluid forces acting on the active section could be calculated by subtracting the output of the load cell inside the dummy section from that of the load cell inside the active section. The sensitiveness of the load cell was $7.58\,\mathrm{mV\,g^{-1}}$. More details of the load cells and fluid force measurement could be found in Alam *et al.* (2002, 2005) and Sakamoto & Oiwake (1984). The end effects on the measured force were negligibly small, as the force measurements were made only on the instrumented midsection of $1.07d$ in length. The geometric blockage and cylinder length-to-width (aspect) ratios in the test section, were $3.5\,\%$ and 7, respectively. No corrections were made to compensate the blockage effect; the possible effects of the blockage and aspect ratio are given in §4.

Two single hot wires were placed at $x/d = 3$ and $y/d = \pm(0.5T/d + 1.5)$, respectively, in a plane through the midspan of the cylinders to measure simultaneously the streamwise velocity fluctuations u_1 and u_2 behind each of the two cylinders, which were used to determine the frequencies of vortex shedding from the cylinders (figure 1). The load-cell- and hot-wire-measured analogue signals were amplified, digitalized at a sampling frequency of 1.5 kHz and then processed using a microcomputer (NEC PC $=$ 9801F) and a data processor (NEC-SANEI 'T17S). At least three sets of signals were captured for a duration of about 10 s for each T/d. Fourier power spectral density, co-spectra and coherence of the hot-wire signals were determined on the basis of the average of 14 runs, each composed of $1024\,(2^{10})$ samples.

2.2. *Flow structure measurements*

PIV and LIF flow visualization measurements were conducted in a closed-loop low-speed wind tunnel with a $0.6\,\mathrm{m} \times 0.6\,\mathrm{m}$ test section of length 2.4 m. Two square cylinders of $d = 20\,\mathrm{mm}$, made of brass, were arranged side by side and mounted horizontally across the width of the tunnel. Further, U_∞ was $12\,\mathrm{m\,s^{-1}}$, resulting in $Re = 1.7 \times 10^4$. The flow velocity in the test section was uniform to $0.1\,\%$, and the longitudinal turbulence intensity was less than $0.4\,\%$. See Huang, Zhou & Zhou (2006) for more details of the tunnel.

A Dantec PIV system was used to measure the near wake of the cylinders in the (x, y) plane. The flow was seeded with smoke, which was generated from paraffin oil, with particles about $1\,\mu\mathrm{m}$ in diameter. Flow illumination was provided by two New Wave standard pulse laser sources of a 532 nm wavelength, each with a maximum energy output of 120 mJ per pulse. The interval between two successive pulses was $50\,\mu\mathrm{s}$. Each laser pulse lasted for $0.01\,\mu\mathrm{s}$. One charge-coupled device (CCD) camera (HiSense MkII, gain $\times$ 4, double frames, 1344×1024 pixels) was used to capture particle images, covering an area of $x^* = 0.8$ to 10.8 (200 mm) and $y^* = -5.3$ to 5.3 (212 mm). In this paper, the asterisk denotes normalization by d and/or U_∞. Synchronization between image taking and flow illumination was provided by the Dantec FlowMap Processor (PIV2001 type). In image processing, an interrogation window of 32×32 pixels was used with $25\,\%$ overlap in each direction. The ensuing in-plane velocity fields consisted of 54×56 vectors, which produced the same number of vorticity data. About 800 images were captured for $T/d = 1.02$, 3.50 and ∞ (single cylinder). The number of images was increased to about 2000 for $T/d = 1.12$, 1.75 and 5.0, where multiple flow modes occurred. When the flow was subjected to multiple modes, the PIV images were sorted, through the visual examination of all images one by one, into different groups based on the flow modes. Each mode of the flow consisted of at least 500 PIV images, which allowed the mean streamwise and lateral velocities ($\overline{U}^*$ and $\overline{V}^*$) and the corresponding r.m.s. velocities (u^*_{rms} and v^*_{rms}) to be estimated. The progressively averaged and r.m.s. values of the streamwise velocity at
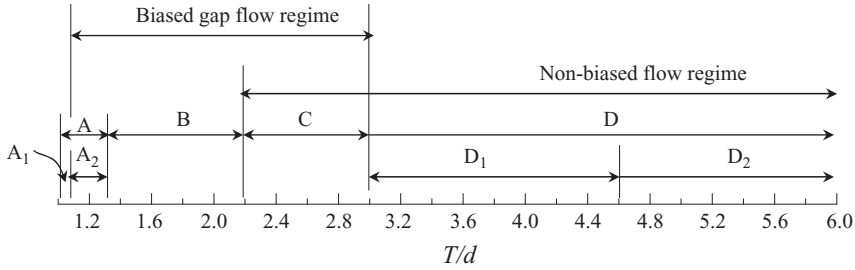
FIGURE 3. Dependence of flow regimes on T/d: A, single-body regime (A_1, perfectly single-body wake; A_2, single-body-like wake); B, two-frequency regime; C, transition regime; D, coupled vortex street (CVS) regime (D_1, anti-phase-dominated vortex shedding; D_2, anti-phase–in-phase mixed vortex shedding).

the point corresponding to the shear layer roll-up position, where the maximum u_{rms} occurs (Alam *et al.* 2010), have been confirmed to approach their asymptotic values when the number of images reached 400. The moving averaged data with a running sample of 500 exhibited an uncertainty of $\pm 3\%$ and $\pm 5\%$ for the mean and r.m.s. velocities, respectively.

   The same PIV system was used for LIF flow visualization under the same flow conditions. Smoke generated from paraffin oil was released from two pinholes 0.75 mm in diameter, drilled at the two leading-edge corners, respectively, at the midspan of the cylinders. The particle images were taken using one of two PIV CCD cameras.

3. Flow structure and classification

3.1. *Classification of flow regimes*

After careful examination of measured fluid forces, St, LIF flow visualization and PIV data, four distinct flow regimes are identified, i.e. the single-body regime (regime A), the two-frequency regime (regime B), the transition regime (regime C) and the CVS regime (regime D). Their corresponding T/d ranges are given in figure 3, and the representative flow structures are shown in figure 4.

   The single-body regime occurs at $T/d < 1.3$, where the two cylinders behave like a single body, and the outer shear layers separate alternately from each cylinder, forming a staggered vortex street (figure 4*b,c*) like that behind a single cylinder (figure 4*a*). The gap flow between the cylinders appears absent at $T/d \leqslant 1.02$ (figure 4*b*) and is appreciably visible for $1.02 < T/d < 1.3$ (figure 4*c*). As will be seen later, this little difference has a rather pronounced impact on fluid forces. As such, regime A may be further subdivided into two; the former is termed as the perfectly single-body regime A_1 and the latter the single-body-like regime A_2. At $T/d = 1.3$–2.2, the gap flow between the cylinders is biased with adequate strength to form one narrow and one wide street (figure 4*d*), which are associated, respectively, with a high and a low St, thus called the two-frequency regime (regime B). The gap flow may switch randomly from one side to the other, resulting in a swap between the narrow and wide streets (figure 4*d₁,d₂*). In the transition regime (regime C, $2.2 < T/d < 3.0$), the two distinct frequencies characterized by regime B collapse into one from time to time, the narrow and wide streets changing (figure 4*e₁,e₃*) accordingly to two anti-phased or symmetric streets of the same frequency (figure 4*e₂*). Therefore, three different flow modes may occur, with the gap flow biased downward (figure 4*e₁*), unbiased (figure 4*e₂*) and biased upward (figure 4*e₃*). Beyond $T/d = 3.0$, vortex shedding from one cylinder is
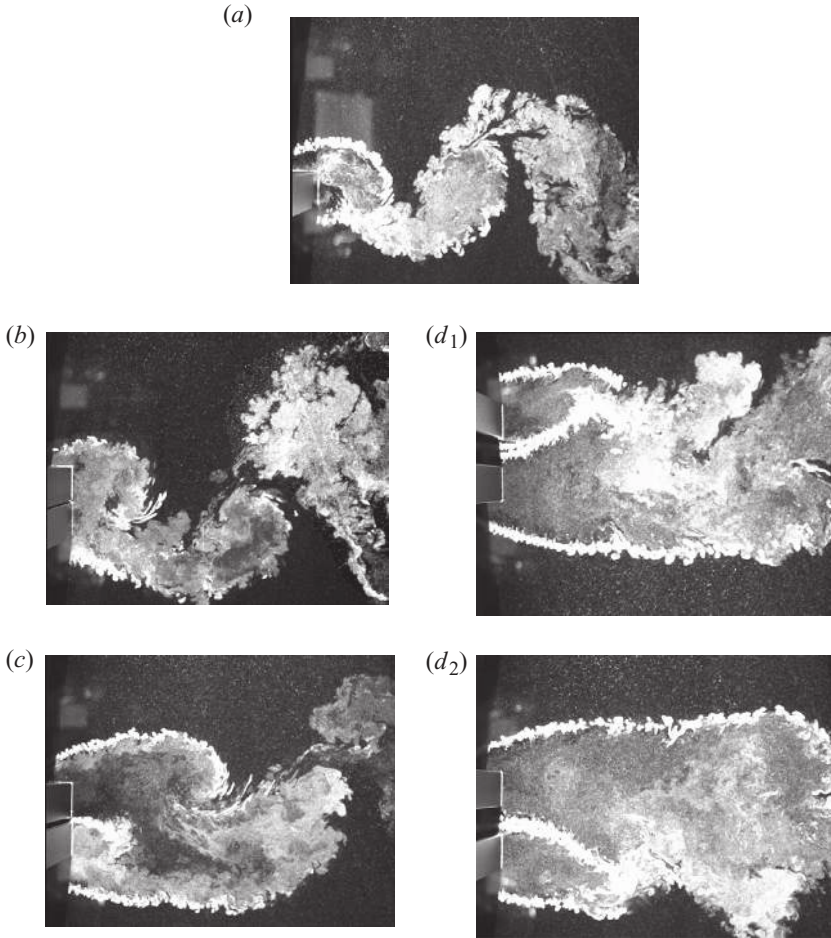
FIGURE 4. See caption on next page.

constantly coupled with that from the other, with their frequencies identical, which is referred to as the CVS regime or regime D (figure 4*f,g*). Depending on the phase shift between the two streets, this regime is further divided into two sub-regimes, namely anti-phase-dominated vortex shedding D_1 ($T/d = 3.0$–4.6), where the two vortex shedding processes are predominantly anti-phased (figure 4*f*), and anti-phase–in-phase mixed vortex shedding D_2 ($T/d = 4.6$–60) where both anti- and in-phased vortex sheddings are frequently observed (figure $4g_1, g_2$).

Remarks are due on the observed bistability and changeover of the gap flow in regime B. On the basis of examining the consecutive images of the LIF flow visualization, Wang & Zhou (2005) investigated the gap flow bistability and changeover in the wake of two side-by-side-arranged circular cylinders ($T/d = 1.7$). They noted that the stable gap flow deflection was in general associated with the amalgamation of three gap vortices: the two cross-stream vortices in the narrow wake were typically engaged in pairing, generating a relatively low-pressure region between them and subsequently drawing in a gap vortex in the wide wake. On the other hand, the gap flow switch was often accompanied by a change in phase between the gap vortices of the two streets, which caused the three vortices to fail
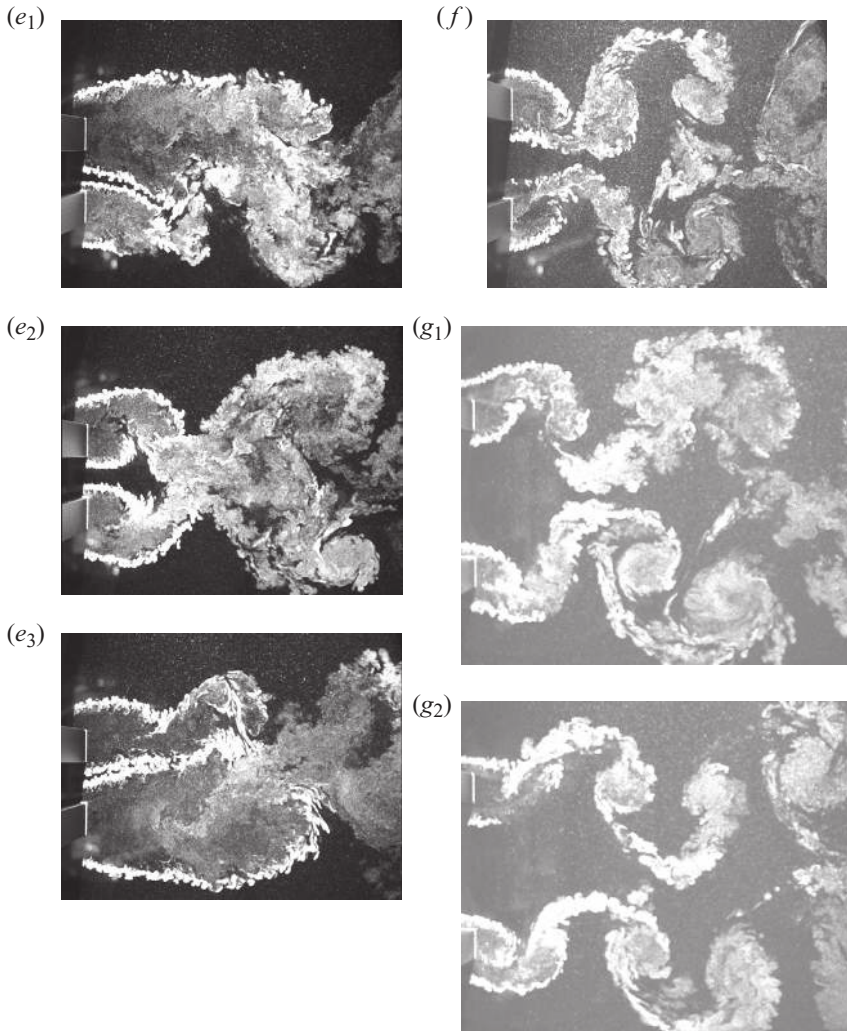
FIGURE 4. Typical photographs from LIF flow visualization. (*a*) A single isolated cylinder wake. Single-body regime: (*b*) regime A_1, perfectly single-body wake ($T/d = 1.02$) without gap flow; (*c*) regime A_2, single-body-like wake ($T/d = 1.12$) with gap flow; the outer shear layers roll up, forming a staggered vortex streak. Two-frequency regime B ($T/d = 1.75$): (d_1) narrow and (d_2) wide streets correspond to higher and lower vortex shedding frequencies, respectively. Transition regime C ($T/d = 2.4$): transition from (e_1) a combination of of narrow and wide streets to (e_2) anti-phased streets and then to (e_3) a different combination of narrow and wide streets, or vice versa. Three distinct dominant frequencies occur. (*f*) Coupled vortex shedding regime D_1 ($T/d = 3.5$): anti-phased vortex shedding. Coupled vortex shedding regime D_2 ($T/d = 5.0$): (g_1) anti-phased and (g_2) in-phased. The same scale has been applied for the photographs to facilitate comparison.

in amalgamation. They argued that the amalgamation of the three gap vortices was at least partially responsible for the stability of the gap flow deflection, and vigorous vortex interactions could also cause the gap flow to switch from one side to another. The LIF flow visualization was presently also conducted in a water tunnel. A similar observation was made when the consecutive images obtained from visualization were examined (not shown). It may be inferred that the physical mechanisms behind the
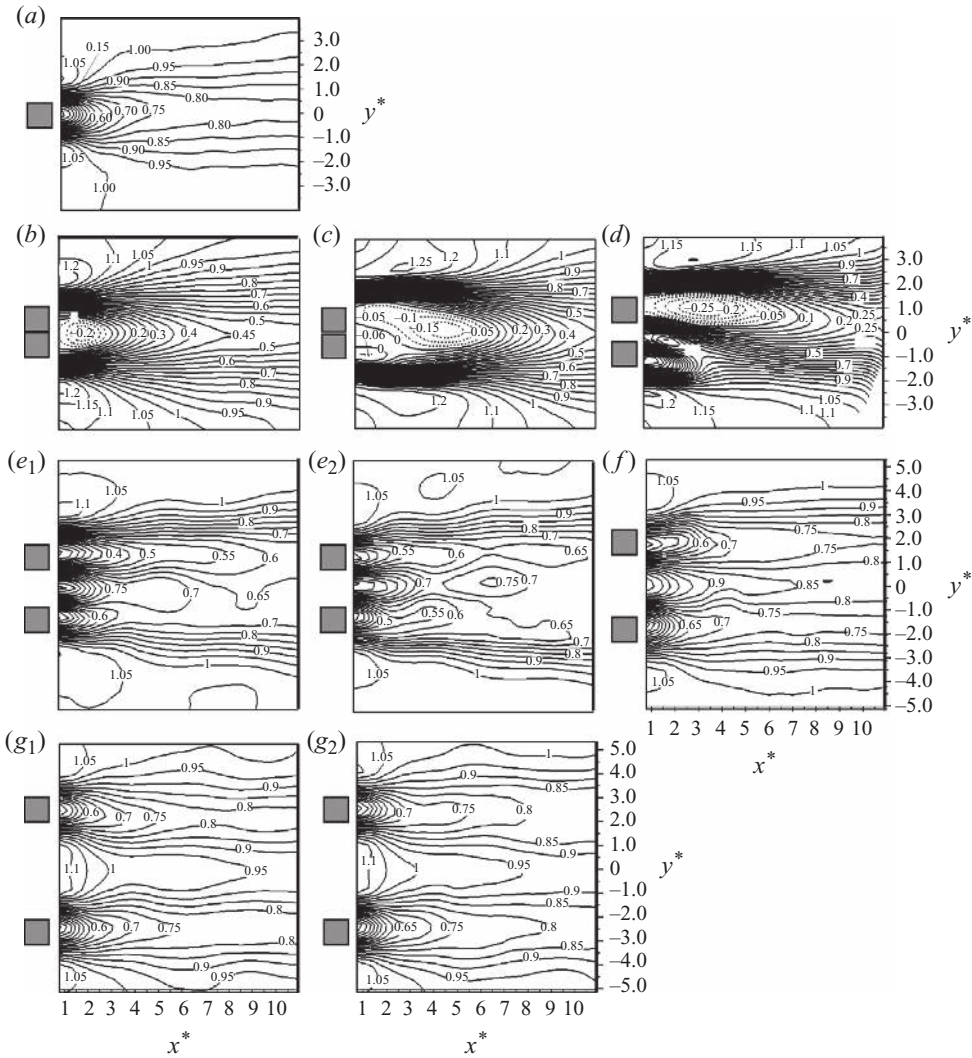
FIGURE 5. Isocontours of the averaged streamwise velocity $\overline{U}^*$ in different regimes: (*a*) single isolated cylinder; (*b*) regime A_1 ($T/d = 1.02$); (*c*) regime A_2 ($T/d = 1.12$); (*d*) regime B ($T/d = 1.75$); (*e*) regime C ($T/d = 2.4$), (e_1) biased downward and (e_2) coupled; (*f*) regime D_1 ($T/d = 3.5$); (*g*) regime D_2 ($T/d = 5.0$), (g_1) anti-phased and (g_2) in-phased. The solid and dotted lines represent positive ($\geqslant 0$) and negative (<0) contour levels, respectively. Contour increment is 0.05.

bistability and changeover of the gap flow in regime B should be the same as their counterparts in the wake of circular cylinders.

3.2. *Velocity field and wake characteristics*

3.2.1. *Streamwise velocities and wake characteristic parameters*

The near-wake characteristics in each flow regime, including the wake width, vortex formation length, recirculation bubble and velocity recovery, may be investigated through examining the isocontours of the time-averaged and r.m.s. velocities, i.e. $\overline{U}^*$ and u^*_{rms}. Figure 5 presents the $\overline{U}^*$-contours in different regimes, along with those in a single isolated cylinder wake. The same increment in the contour level is used to

facilitate comparison. Note that the contours with the gap flow biased only downward are presented for regimes A_2, B and C. The recirculation bubble size, enclosed by $\overline{U}^* = 0$, provides a measure for the strength of recirculation. The recirculation bubble is large for regime A_1 (figure 5b) or A_2 (figure 5c), where the two cylinders act like a single entity, resulting in large effective cylinder width. This is the same for regime B behind the upper cylinder, i.e. in the wide street (figure 5d). In contrast, this bubble is significantly smaller for the narrow street of regime B (figure 5d) and regime D (figure 5f–g_2); so is the single-cylinder wake. Accordingly, $\overline{U}^*$ recovers rapidly in these regimes, reaching 0.7 at $x^* = 3$–5. On the other hand, when the wake consists of two streets of distinct widths, both streets exhibit a slower recovery than the single-cylinder wake, although the narrow one (lower) is associated with a faster velocity recovery than the wide (figure 5d,e_1) one. Note that the velocity recovery is connected to the entrainment of free-stream fluid into the wake (e.g. Alam & Zhou 2007b). As will be shown later, the outer shear layer of the narrow street feeds more free-stream fluid into the wake than that of the wide street, and the gap flow is mostly directed into the narrow street, both contributing to the faster recovery in the narrow street. Another reason of the weaker recovery of the wide street is the presence of its large recirculation area, which requires more fluid to be entrained for the same rate of velocity recovery.

The dynamics of the gap flow between the cylinders plays a crucial role in generating distinct flow regimes. This is reflected in the dependence of the flow regime on the momentum, related to both T/d and $\overline{U}^*$, through the gap. Since $\overline{U}^*$ is not measured presently at $x^* = 0$ in the gap (figure 5), we may examine $\overline{U}^*$ at $x^* = 0.7$, instead, to estimate qualitatively the momentum through the gap. This momentum is very small, in fact with a negative $\overline{U}^*$ at $x^* = 0.7$ (figure 5b,c) in regime A, naturally its effect on the wake being negligible and a single street occurring. It increases appreciably in regime B, with the maximum $\overline{U}^* > 0.6$ at $x^* = 0.7$ (figure 5d), though not enough to force the flow through the gap without being biased, producing two streets of distinct widths. With the two cylinders symmetrical with respect to the incident flow, the probability for the gap flow to be biased towards either of the two sides is supposed to be the same as the other, and the gap flow switches rather randomly from one side to the other. In regime C, with the maximum $\overline{U}^* > 1.0$ at $x^* = 0.7$ (figure 5e_1,e_2), the momentum through the gap gains such a strength that approaches to be adequate to maintain an unbiased gap flow. As such, the gap flow manages to be straight intermittently, generating the CVS flow mode as well as the biased modes. In regime D, the momentum through the gap is adequately large to maintain an unbiased gap flow all the time, with the biased modes disappeared.

Figure 6 compares the u^*_{rms}-contours in different regimes. A number of observations can be made. Firstly, the maximum u^*_{rms} that occurs in general at the shear layer roll-up position (Bloor 1964; Gerrard 1966) is very high (0.39–0.4) at $T/d = 1.02$ (regime A_1), then drops as T/d increases to 1.75 (regime B) and rebounds for further increasing T/d. Secondly, the wide street in regime B has a higher maximum u^*_{rms} associated with the outer shear layer than the narrow street (figure 6d,e_1), implying a higher strength of vortices in the wide street. Thirdly, the inner shear layers are characterized by a larger maximum u^*_{rms} than the outer ones (figure 6d–g_2). Fourthly, in the case of the biased gap flow (figure 4d–e_2; regimes B and C), the two inner shear layers, though producing oppositely signed vortices, correspond to only one peak in the u^*_{rms}-contours (figure 6d–e_2). Similarly, in the CVS regime of small T/d, say at 2.4 (figure 6e_2), the two inner shear layers, albeit considerably separated (figure 4e_2),
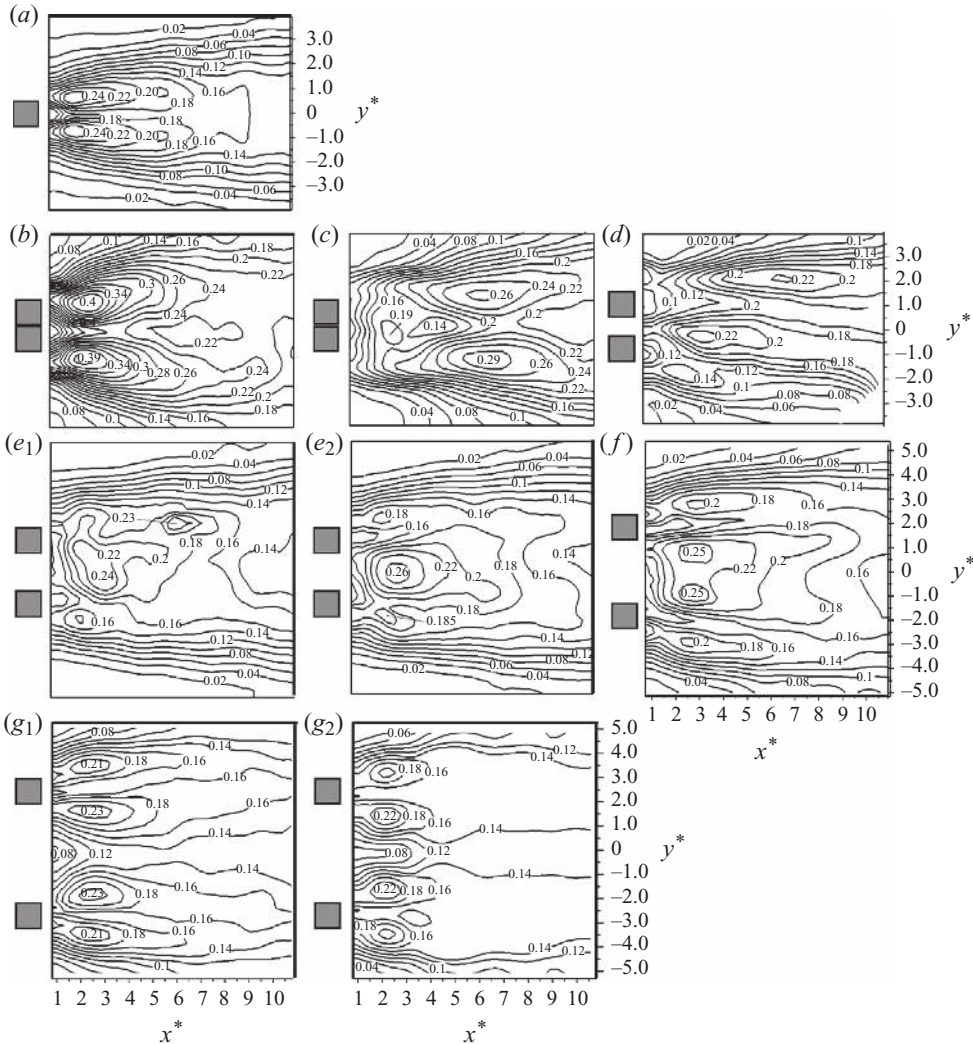
FIGURE 6. Isocontours of the r.m.s. streamwise velocity u^*_{rms}: (*a*) single isolated cylinder; (*b*) regime A_1 ($T/d = 1.02$); (*c*) regime A_2 ($T/d = 1.12$); (*d*) regime B ($T/d = 1.75$); (*e*) regime C ($T/d = 2.4$), (e_1) biased downward and (e_2) CVS; (*f*) regime D_1 ($T/d = 3.5$); (*g*) regime D_2 ($T/d = 5.0$), (g_1) anti-phased and (g_2) in-phased. Contour increment is 0.02.

produce only one peak at $y^* = 0$, which is connected to the oscillation or the roll-up of the inner shear layers. Fifthly, in-phased vortex shedding from the two cylinders, though producing the same maximum u^*_{rms} (0.21–0.23) as the anti-phased vortex shedding (figure $6g_1, g_2$), is associated with a more rapid downstream decay in u^*_{rms}; that is, the in-phased vortices are less stable than the anti-phased ones, as concluded by Zhou, Zhang & Yiu (2002). The maximum u^*_{rms} (0.21–0.23) in this regime is close to that (0.24) in a single isolated cylinder wake. Finally, a small peak with a magnitude of 0.19 at $x^* = 2.3$ and $y^* = -0.4$ (figure 6*c*) is probably connected to the gap flow rolling up near the base of the cylinders (figure 4*c*).

The wake width w and the vortex formation length L_f are two important characteristic parameters of a wake. The former is defined as the transverse separation
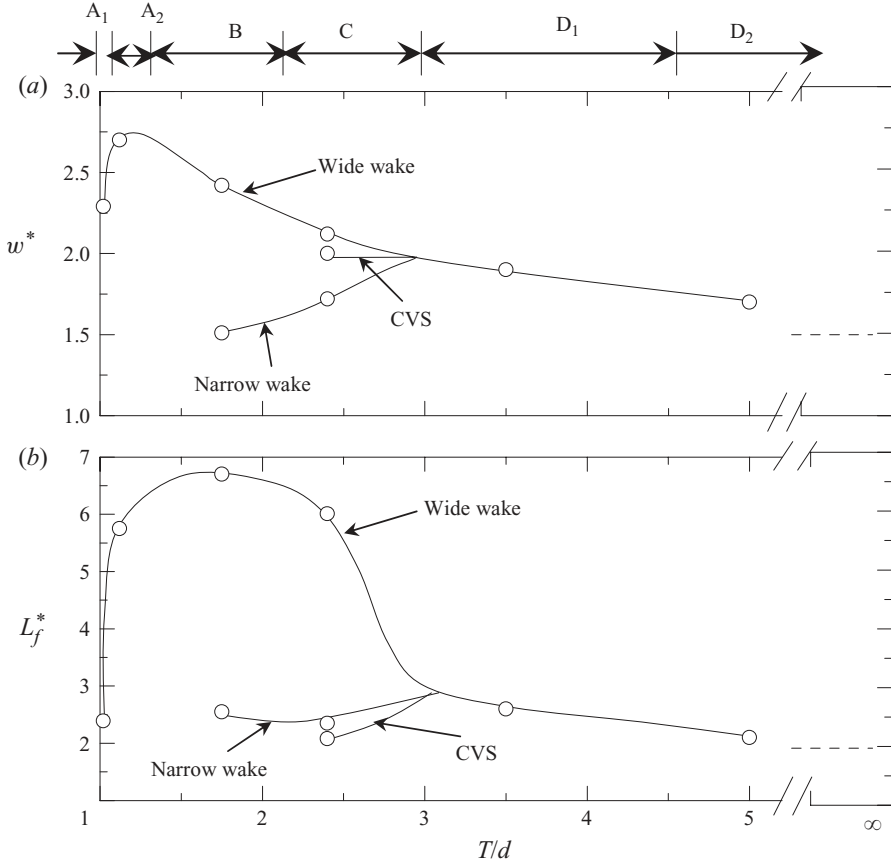
FIGURE 7. Dependence on T/d of (a) the wake width (w^*) and (b) the vortex formation length (L_f^*). The dashed line denotes a single isolated cylinder ($T/d = \infty$).

between the free shear layers in the wake (e.g. Roshko 1954). An alternative definition is the transverse separation between the two maxima in the u_{rms}^*-contours (Griffin & Ramberg 1974; Ramberg 1983), which has been widely used (e.g. Roshko 1993; Balachandar, Mittal & Najjar 1997; Paranthoen *et al.* 1999; Alam & Zhou 2007b). This width is linked with the fluid forces on the wake generator. A large w corresponds to a small base pressure (Nakaguchi, Hasimoto & Muto 1968), low St and large C_D. Moreover, L_f is defined as the streamwise distance of the maximum u_{rms}^* from the cylinder axis (Bloor 1964; Gerrard 1966). Both parameters can be estimated from the PIV-measured u_{rms}^*-contours. Figure 7 presents the dependence of w^* and L_f^* on T/d. The values of w^* and L_f^* are about 2.3 and 2.4, respectively, at $T/d = 1.02$ (sub-regime A_1), but grow rapidly from $T/d = 1.02$ to $T/d = 1.12$ (sub-regime A_2). This difference between A_1 and A_2 results from the occurrence of a thin gap flow in A_2, which acts as a base bleeding, prolonging L_f^* and reducing the curvature of the outer shear layers, as is evident in figures 4(*b,c*) and 5(*b,c*). The observation suggests a pronounced effect of the gap flow between two cylinders on the near-wake dynamics. The reduced curvature leads to a larger w^* (figure 7). With an increasing strength in the gap flow in regime B (figure 4*d*), the curvature is further decreased (figure 5*d*). Subsequently, L_f^* of the wide street grows further, reaching a maximum of 6.7 at $T/d = 1.75$; the corresponding L_f^* of the narrow street is 2.7. Accordingly, the narrow

and wide streets correspond to $w^* = 1.5$ and 2.4, respectively, at $T/d = 1.75$, smaller than in regime A_2. As T/d increases from regime B to C, both w^* and L_f^* diminish significantly for the wide street but increase for the narrow street, which is ascribed to a less biased gap flow. The CVS mode in regime C corresponds to an intermediate w^* between those of the wide and narrow streets and an L_f^* smaller than that of the narrow street. With increasing T/d, both w^* and L_f^* in regime D retreat and approach their counterparts ($w^* = 1.5$, $L_f^* = 2.0$) of a single isolated cylinder wake, implying a diminishing interference between the streets.

3.3. *Lateral velocities and entrainment*

Insight into entrainment of ambient fluid into the wake as well as the vortex formation and forces on the cylinders may be gained by examining the $\overline{V}^*$-contours and v_{rms}^*-contours in different regimes (figures 8 and 9). In the single isolated cylinder wake (figure 8a), the positive and negative $\overline{V}^*$-contours display the same maximum magnitude at $y^* = \pm 0.93$ and occur below and above the centreline ($y^* = 0$), respectively. The observation suggests that the velocity at which the ambient fluid on the lower side is entrained into the wake is accelerated up to $y^* \approx -0.93$ and then decelerated until $y^* = 0$. A similar remark may be made for the entrainment of ambient fluid on the upper side ($y^* > 0$). At $T/d = 1.02$ (regime A_1), the $\overline{V}^*$-contours display the qualitatively same twin-peak pattern for $x^* > 1.5$ as the single-cylinder wake. The region of $x^* < 1.4$ displays the positive and negative contours on the upper and lower sides, respectively. Such a region is absent in the single-cylinder wake. Two factors are responsible for the observation. Firstly, as the recirculation region is blocked on the left side by the cylinder rear surface and the reversed mass flow must be conserved, the reversed flow is diverted upward and downward, respectively, engendering the positive and negative $\overline{V}^*$ near the base or the region of $x^* < 1.4$ and $y^* = -1$ to 1. Secondly, the outer shear layers, separated from the cylinder but not rolled up yet, result in the positive and negative contours in the regions of $x^* < 1.4$–3 (depending on y^*) and $y^* > \pm 1$, respectively. The twin peaks in the $\overline{V}^*$-contours are shifted further downstream in sub-regime A_2 (figure 8c) as L_f^* is prolonged. The downward-biased gap flow generates a negative peak of -0.11 at $(x^*, y^*) = (2.4, -1)$. The peak below the centreline has a larger magnitude than that above the centreline; that is, the lower outer shear layer brings in more free-stream fluid into the wake than the upper outer shear layers, which contributes to the larger velocity recovery in the narrow street, as discussed earlier. In regime B (figure 8d), the two peaks that occur at $(x^*, y^*) = (2.2, -2)$ and $(2.2, -0.5)$, respectively, are connected to the lower narrow street, whilst those at $(x^*, y^*) = (7.2, 2.5)$ and $(5.0, 0.0)$ are associated with the upper wide street (see figure 4d_2). Each street in the CVS mode shows the $\overline{V}^*$-contours (figure 8e_2–g_2) qualitatively similar to those of the single isolated cylinder wake. Note that, because of the biased gap flow, the negative $\overline{V}^*$-contours overwhelm the positive ones in the near wake ($x^* < 4$) for regimes A_2, B and C. This could have a significant impact on both the sign and the magnitude of C_L on the cylinders, as will be discussed later.

The v_{rms}^*-contours display one peak on the centreline in the single-cylinder wake (figure 9a). So do those in regime A (figures 9b,c). The contours show two peaks in other regimes (figure 9d–g_2), which are staggered in regime B (figure 9d) and the two-frequency mode of regime C (figure 9e_1), owing to two different vortex formation lengths in the two streets. The magnitude of the peak is smallest in regime B, suggesting a smallest C_L', as confirmed later.
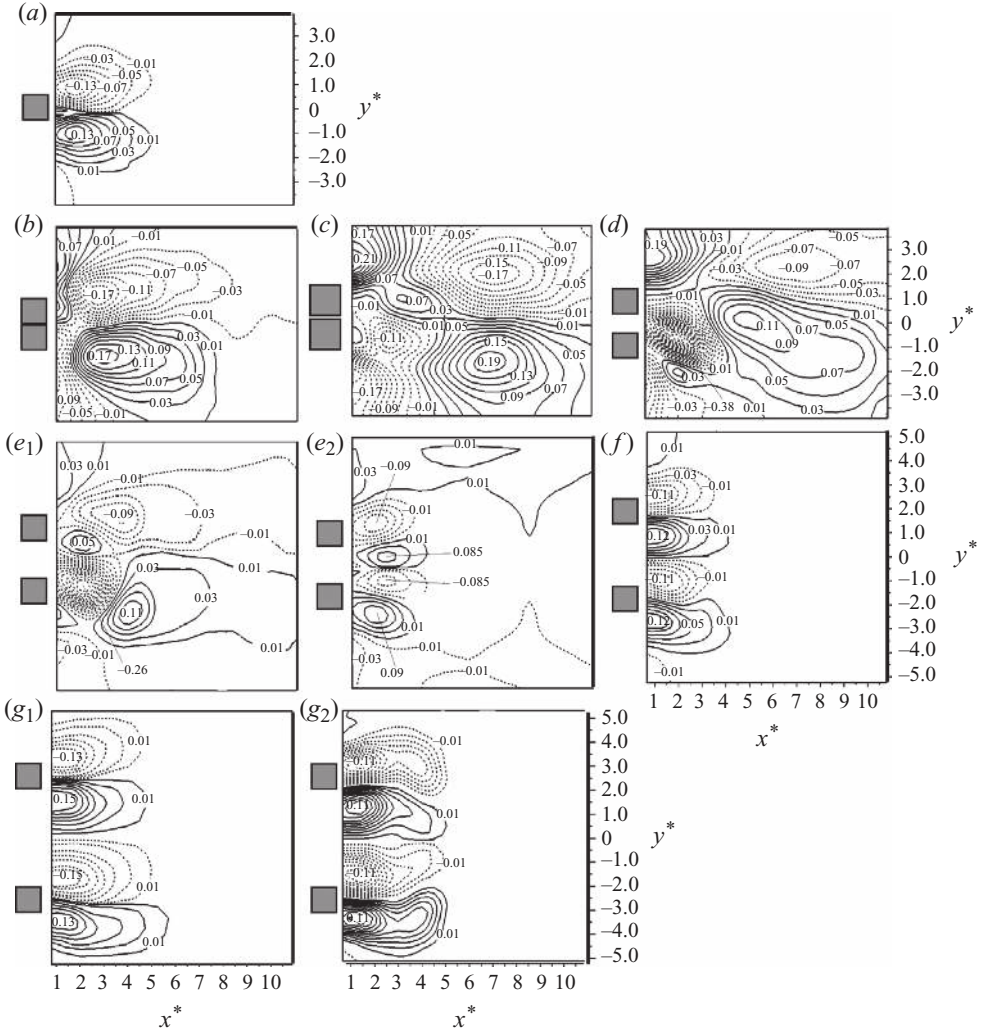
FIGURE 8. Isocontours of the averaged lateral velocity $\overline{V}^*$: (*a*) single isolated cylinder; (*b*) regime A_1 ($T/d = 1.02$); (*c*) regime A_2 ($T/d = 1.12$); (*d*) regime B ($T/d = 1.75$); (*e*) regime C ($T/d = 2.4$), (e_1) biased downward and (e_2) coupled; (*f*) regime D_1 ($T/d = 3.5$); (*g*) regime D_2 ($T/d = 5.0$), (g_1) anti-phased and (g_2) in-phased. The solid and dotted lines represent positive ($\geqslant 0$) and negative (< 0) contour levels, respectively. Contour increment is 0.02.

4. Validation of force and St measurements

In order to provide a validation for the present measurement techniques, a single isolated square cylinder wake was measured in terms of steady and unsteady fluid forces and the Strouhal number, which are known to be insensitive to Re in the subcritical flow regime, especially for $Re > 500$ (Okajima 1982; Norberg 1993). Table 1 compares presently measured C_{D0}, C'_{D0}, C'_{L0} and St_0 with those available in the literature, where the subscript 0 denotes the dimensionless quantities in the single isolated square cylinder wake. The deviation between the present St, 0.128, and others is quite small. Further, St, C_D, C'_D and C'_L are all dependent on experimental conditions such as the turbulent intensity, blockage, aspect ratio and end effects (Surry

Research	Re	Blockage, aspect ratio	Turbulent intensity	Force measurement technique	C_{D0}	C'_{D0}	C'_{L0}	St_0
Novak (1974)	5×10^3–1.5×10^4	2.52 %, 13	2.2 %	–	–	–	–	0.138
Nakaguchi et al. (1968)	2×10^4–7×10^4	–	Smooth	Sectional (pressure distribution)	2.1	–	–	0.13
Bearman & Trueman (1972)	6.8×10^4		Smooth	Sectional (pressure distribution)	2.19			0.13
Lee (1975) Lee (1975)	1.76×10^5	3.6 %, –	0.5 %	Sectional (pressure distribution)	2.20	0.23	1.2	0.12
Reinhold et al. (1977)	1.4×10^6	5.6 %, 17	12 %	Sectional (pressure distribution)	2.19	0.23	1.07	0.13
Courchesne & Laneville (1982)	6×10^4	Corrected, 22	Smooth	On the full length, 22d (load cell)	2.22	–	–	–
	5×10^4	Corrected, 22	0.6 %		2.22	–	–	–
	5×10^4	Corrected, 22	7.4 %		1.87	–	–	–
	5×10^4	Corrected, 22	13.5 %		1.64	–	–	–
Okajima (1982)	10^4–12×10^4	5 %, 13	0.5 %	–	–	–	–	0.13
Bearman & Obajasu (1982)	4.7×10^4	–, 17	Smooth	Sectional (pressure distribution)			1.3	0.125

TABLE 1. Continued.

Research	Re	Blockage, aspect ratio	Turbulent intensity	Force measurement technique	C_{D0}	C'_{D0}	C'_{L0}	St_0
Lesage & Gartshore (1987)	3.3×10^4	4.1 %, 18	–	Sectional (pressure distribution)	2.04	–	1.33	0.13
Sakamoto *et al.* (1987)	5.52×10^4	9.8 %, 9.5	0.19 %	On $1.07d$ (load cell)	2.38	0.18	1.23	0.13
Knisely (1990)	2.2×10^4 4.4×10^4	5 %, 12	0.5 %	On the full length, $12d$ (load cell)	2.05		1.0	0.13
Norberg (1993)	1.3×10^4	4.7 %, 51	Smooth	Sectional (pressure distribution)	2.16	–	–	0.132
Igarashi (1997)	3.2×10^4	20 %, 13	0.4 %	Sectional (pressure distribution)	2.27			0.138
Tamura & Miyagi (1999)	3×10^4	5 %, 6	0.5 %	On the full length, $6d$ (load cell)	2.1		1.05	0.128
Nakagawa, Nitta & Senda (1999)	3×10^3	5 %, 35	0.6 %	–	–	–	–	0.13
Noda & Nakayama (2003)	6.89×10^4	4 %, 10	0.2 %	Sectional (pressure distribution)	2.164	0.21	1.18	0.131
Venugopal *et al.* (2006)	10^4–10^5	3.2 %, 13	Smooth	$0.67d$ (load cell)	2.17	–	–	–
Oudheusden *et al.* (2008)	2×10^4	7 %, 12	Smooth	PIV, momentum method	2.18	–	–	–
Present measurement	4.7×10^4	3.5 %, 7	0.5 %	On $1.07d$ (load cell)	2.15	0.27	1.18	0.128

TABLE 1. A collection of aerodynamic characteristics data in a single-cylinder wake: time-averaged drag (C_{D0}), fluctuating drag (C'_{D0}), fluctuating lift (C'_{L0}) and Strouhal number (St_0). Smooth flow refers to the case with a turbulent intensity of less than 0.2 %.
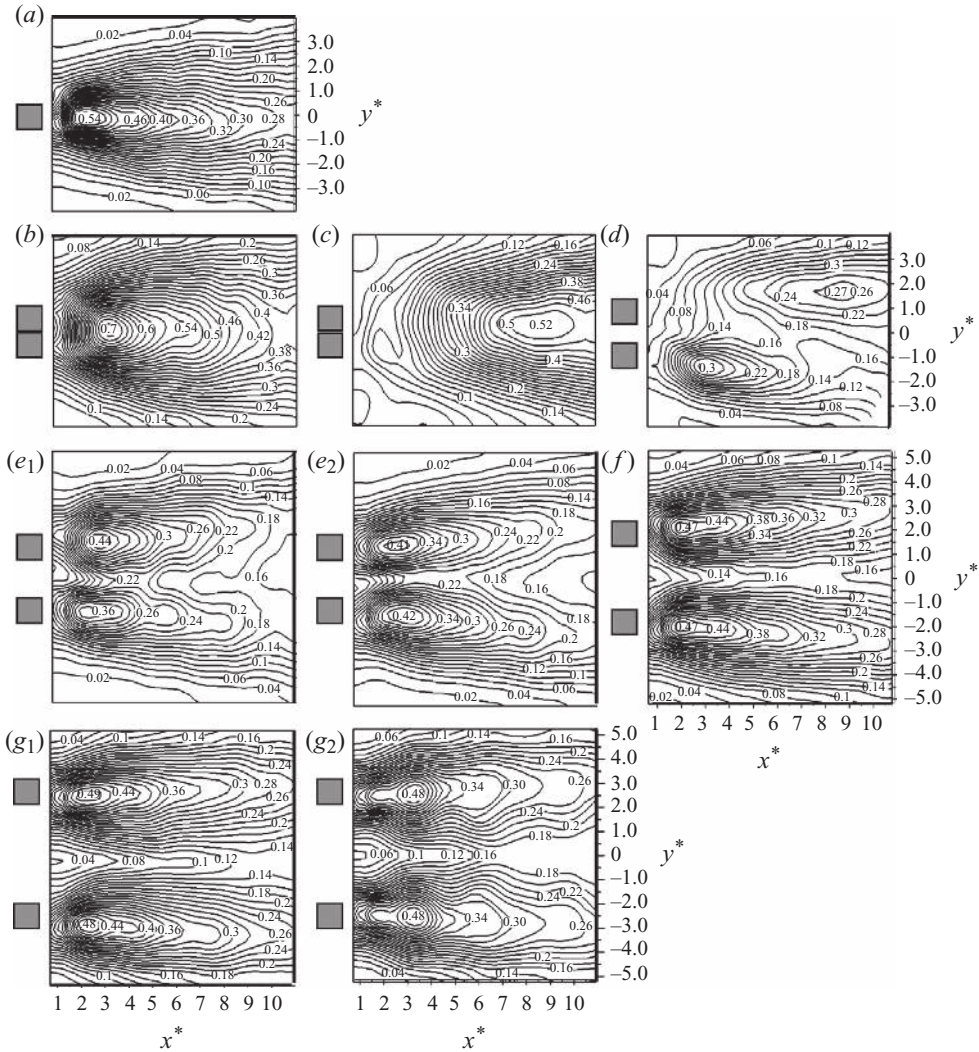
FIGURE 9. Isocontours of the r.m.s. lateral velocity v^*_{rms}: (a) single isolated cylinder; (b) regime A_1 ($T/d = 1.02$); (c) regime A_2 ($T/d = 1.12$); (d) regime B ($T/d = 1.75$); (e) regime C ($T/d = 2.4$), (e_1) biased downward and (e_2) coupled; (f) regime D_1 ($T/d = 3.5$); (g) regime D_2 ($T/d = 5.0$), (g_1) anti-phased and (g_2) in-phased. Contour increment is 0.02.

1972; Laneville, Gartshore & Parkinson 1975). Therefore, a scattering in the data is not unexpected.

The blockage was presently 3.5% for the single-cylinder wake and 7% for two cylinders. The blockage has virtually no effect on C_D if it is less than 6% and may have a very small effect if it is between 6% and 7% (Farell *et al.* 1977; West & Apelt 1982). Therefore, the present blockage (7%) is expected to have a negligibly small effect on C_D. An increased turbulent intensity may lead to a reduced C_D (Courchesne & Laneville 1982) and an increased St (Novak 1974; Okajima 1982). The present C_D, 2.15, agrees well with previous reports: 2.1 by Nakaguchi *et al.* (1968) and Tamura & Miyagi (1999); 2.19 by Bearman & Trueman (1972) and Reinhold, Tieleman & Maker (1977); 2.20 by Lee (1975); 2.16 by Norberg (1993); 2.164 by Noda & Nakayama

(2003); 2.17 by Venugopal, Varyani & Barltrop (2006); and 2.18 by Oudheusden *et al.* (2008). The maximum deviation is less than 2.3%.

The cylinder aspect ratio, i.e. the length-to-width ratio, largely influences C'_D and C'_L. There is relatively large scattering in C'_L, which is highly sensitive to the measurement length of the cylinder (West & Apelt 1997). Furthermore, C'_L is largest when measured at an elemental section, usually from the pressure distribution, and decreases with an increasing measurement length. West & Apelt (1993) demonstrated that, if exceeding 10, the aspect ratio would have no effect on C'_D and C'_L on an elemental section; that is, the 'long' cylinder conditions would hold. The measurements of Szepessy & Bearman (1992) indicated that C'_L on a cylinder with an aspect ratio of 7 was about 2% higher than that with an aspect ratio of 10. Given a turbulent intensity of less than 0.5%, C'_L falls in the range of 1.18–1.33 if measured on a length of less than $1.07d$ (Lee 1975; Bearman & Obajasu 1982; Lesage & Gartshore 1987; Sakamoto, Haniu & Obata 1987; Noda & Nakayama 2003) and in the range of 1.0–1.07 if measured on a full length of $6d$–$12d$ (Knisely 1990; Tamura & Miyagi 1999). The present $C'_L = 1.18$ on a length of $1.07d$ is comparable to those (1.18 and 1.2) reported by Noda & Nakayama (2003) and Lee (1975), whose experimental conditions were almost the same as the present. Nevertheless, the present C'_D, 0.27, is slightly higher than that of previous reports (0.18–0.23).

The above comparison provides a validation for present measurements.

5. Spectral signatures of vortices and Strouhal numbers

The predominant frequencies of vortices generated by the two cylinders and their interrelationship may be extracted from the power spectral density functions E_{u_1} and E_{u_2} (figure 10) of the simultaneously measured u_1 and u_2 (§2.1, figure 1), co-spectrum $Co_{u_1u_2}$ (figure 11), spectral coherence $Coh_{u_1u_2}$ ($\equiv (Co^2_{u_1u_2} + Q^2_{u_1u_2})/E_{u_1}E_{u_2})$) (figure 12) and phase shift $\phi_{u_1u_2}$ ($\equiv \tan^{-1}(Q_{u_1u_2}/Co_{u_1u_2})$) (figure 13) between u_1 and u_2, where $Q_{u_1u_2}$ stands for the quadrature spectrum between u_1 and u_2.

The dimensionless frequencies corresponding to the pronounced peaks, marked in figure 10, are replotted as a function of T/d in figure 14(*a*). A single pronounced peak occurs in regime A at $St = 0.07$, 0.067 and 0.063 for $T/d = 1.02$, 1.1 and 1.2, respectively; that is, vortices are separated at the same frequency from the outer sides of the two cylinders (figure 4*b,c*). Corresponding to this peak, a pronounced peak of negative sign occurs in $Co_{u_1u_2}$ (figure 11), and ϕ_{12} is close to $-180°$ (figure 13), indicating that the outer shear layers form vortices alternately for these T/d values. The strength of vortices is strongest at $T/d = 1.02$, where the peak is the most pronounced. Considering the two cylinders as one single entity, the effective St based on the total height ($T + 2d$) is estimated to be 0.141, 0.141 and 0.139, respectively, slightly exceeding 0.138 (Knisely 1990; Norberg 1993) in the wake of a rectangular cylinder with a width-to-height ratio of $W/H = 0.5$, where W and H are the longitudinal and lateral widths of the rectangular cylinder. Our slightly higher St at $d/(T + 2d) < 0.5$ conforms to the observation that a decreasing W/H ($\leqslant 1.0$) will produce an increase in St (Nakaguchi *et al.* 1968). As noted in §3, a biased gap flow occurs at $T/d = 1.1$–1.2 (figures 3 and 4*c*). However, with a small gap width and hence a small amount of flow, the biased gap flow does not have enough strength to divide the wake into two streets and to differentiate the two outer-shear-layer roll-up frequencies.

The peaks corresponding to the vortex shedding frequencies are less pronounced at $T/d = 1.3$–2.2 (regime B) than at $T/d = 1.02$; the gap flow gains considerable
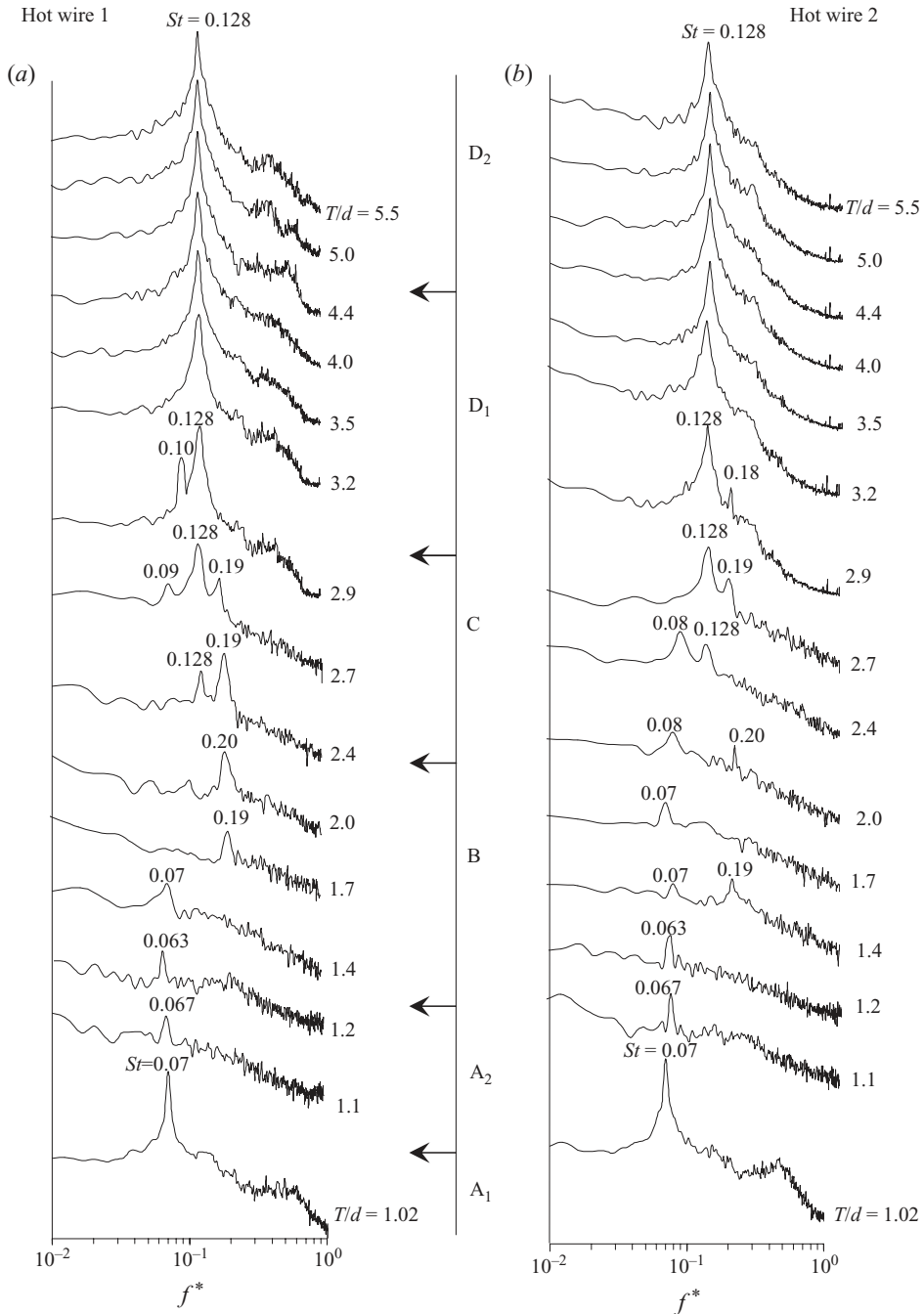
FIGURE 10. The power spectral density functions E_{u1} and E_{u2} of the streamwise fluctuating velocities u_1 and u_2, captured simultaneously from the two hot wires: (*a*) hot wire 1 and (*b*) hot wire 2.

strength and is biased, resulting in the formation of one narrow and one wide street (figure 4d_1,d_2). Two distinct St values occur, with the lower at 0.07–0.08 and the higher at 0.19–0.20; subsequently, no pronounced peak is evident in figures 11 and 12. At $T/d = 2.2$–3.0 (regime C), E_{u_1} and E_{u_2} (figure 10) display one more
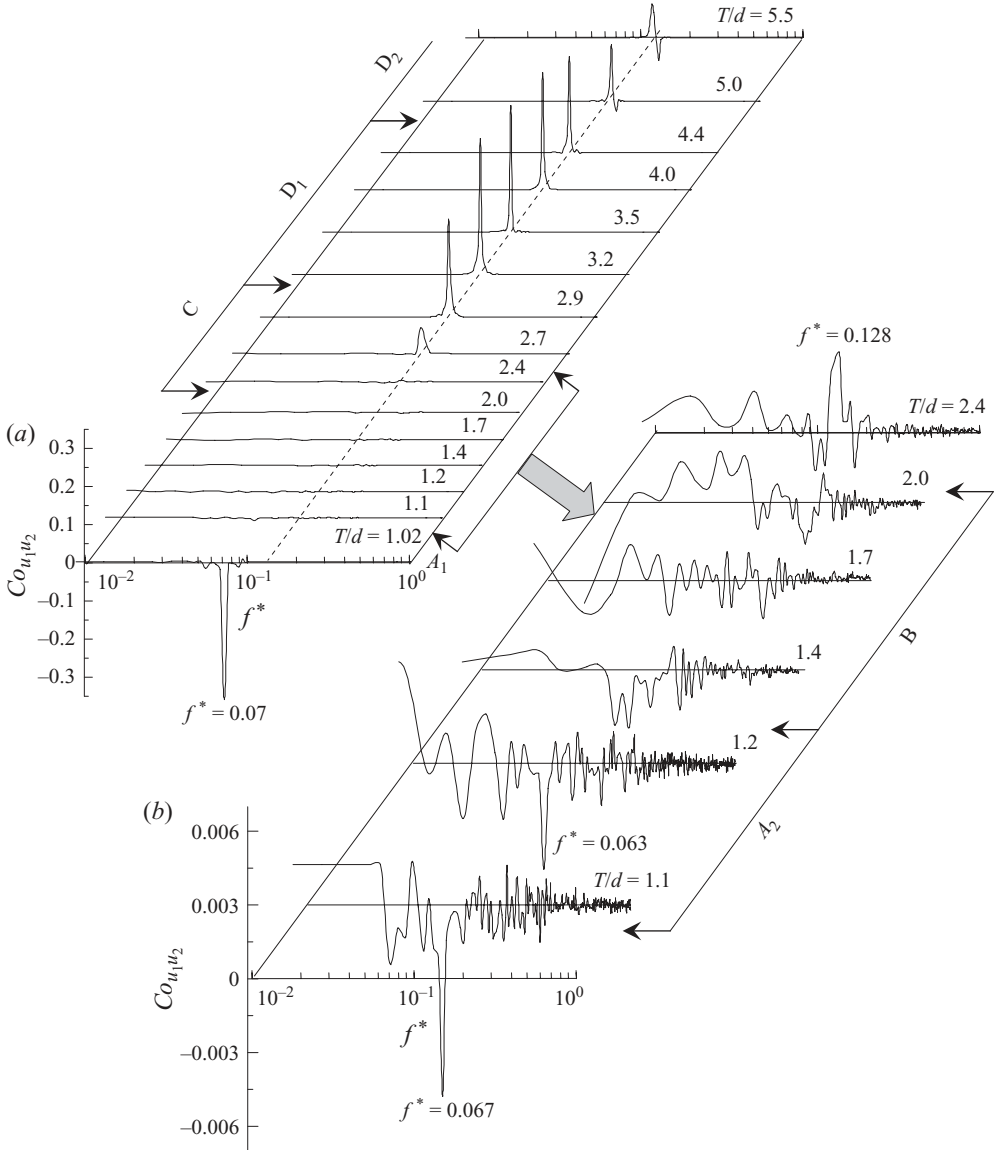
FIGURE 11. (*a*) The co-spectra between u_1 and u_2, captured simultaneously from the two hot wires. (*b*) The amplified co-spectra for $T/d = 1.1$–2.4. The dashed line in (*a*) corresponds to $f^* = 0.128$.

pronounced peak at $St = 0.128$ between the two observed in regime B, internally conforming to the observation of three distinct flow modes (figure $4e_1$–e_3). In the wake of two side-by-side circular cylinders, Ishigai *et al.* (1972, $Re = 1.5 \times 10^3$), Bearman & Wadcock (1973, $Re = 2.5 \times 10^4$), Kamemoto (1976, $Re = 3.0 \times 10^4$), Kim & Durbin (1988, $Re = 3.3 \times 10^3$), Kiya *et al.* (1980, $Re = 2.0 \times 10^4$), Alam *et al.* (2003*a*, $Re = 5.5 \times 10^4$) and Xu *et al.* (2003, $Re = 0.3 \times 10^3$–1.43×10^4) observed two distinct St values for T/d between 1.3–1.5 and 2.0–2.5. The T/d range, depending on Re, is significantly smaller than that ($T/d = 1.3$–3.0) for two side-by-side square cylinders.
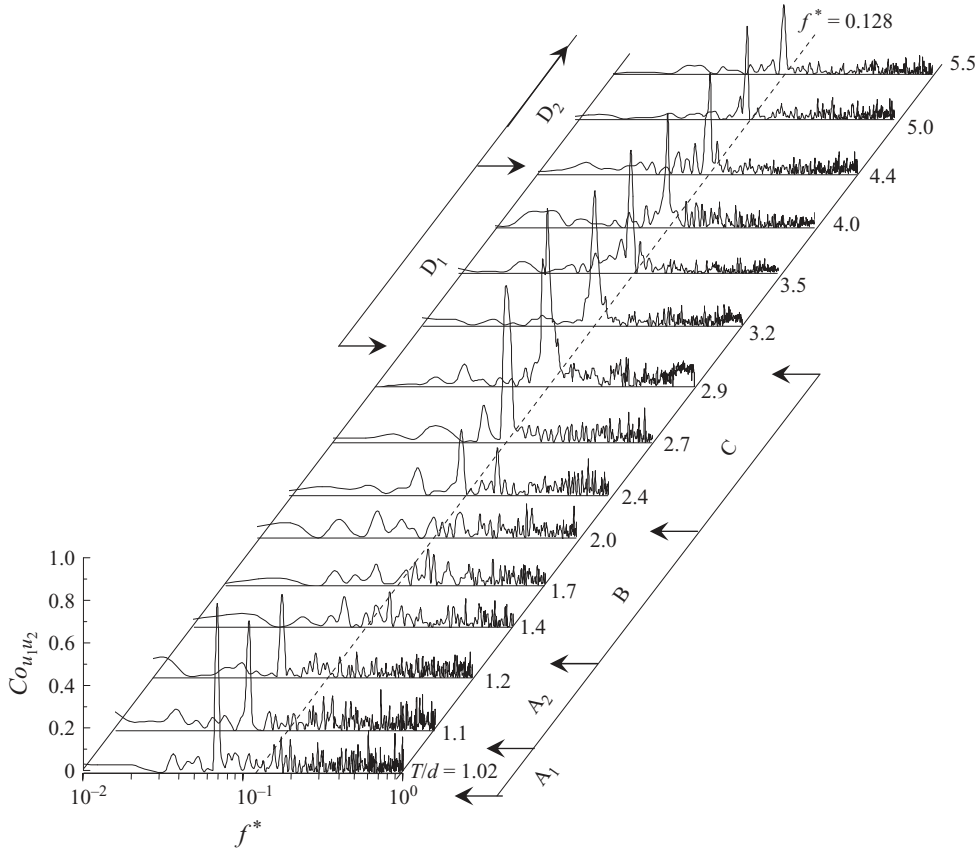
FIGURE 12. Spectral coherence between u_1 and u_2, captured simultaneously from the two hot wires.

Note that the intermediate St, detected in both E_{u_1} and E_{u_2}, is the same as that in regime D (figure 10). The corresponding prominent peak in $Co_{u_1 u_2}$ (figure 11a) is positive and $\phi_{u_1 u_2}$ is close to zero at $St = 0.128$ (figure 13). The observations suggest that the two cylinders generate two synchronized vortex streets of the same frequency with zero phase shift, i.e. two anti-phased streets. Furthermore, the corresponding peak magnitude in $Co_{u_1 u_2}$ and also in $Coh_{u_1 u_2}$ (figure 12) grows gradually from $T/d = 2.2$ to $T/d = 3.0$, implying that the anti-phased CVS flow structure that prevails in sub-regime D_1 starts to emerge, albeit intermittently and gradually, in regime C. As such, this regime is a transition from the two-frequency regime to the CVS regime. At $T/d > 3.0$ (regime D), the same St (0.128) occurs in both streets (figures 10 and 14a), which is equal to St_0 in a single isolated cylinder wake; that is, the two cylinders are adequately separated to generate vortices independently in terms of St. A negative peak is observed at close proximity to the positive peak for $T/d \geqslant 5.0$ in $Co_{u_1 u_2}$ (figure 11a); there is a sudden jump in ϕ_{12} from $0°$ to $180°$ about the arrow (figure 13l,m), the two ϕ_{12} values corresponding to the positive and negative peaks, respectively. The results reconfirm the occurrence of both in- and anti-phased vortex sheddings from the two cylinders, as observed from flow visualization (figure 4g_1,g_2). Kamemoto (1976, $Re = 3 \times 10^4$) and Alam *et al.* (2003a, $Re = 5.5 \times 10^4$) showed in a two side-by-side circular cylinder wake that vortex shedding from the
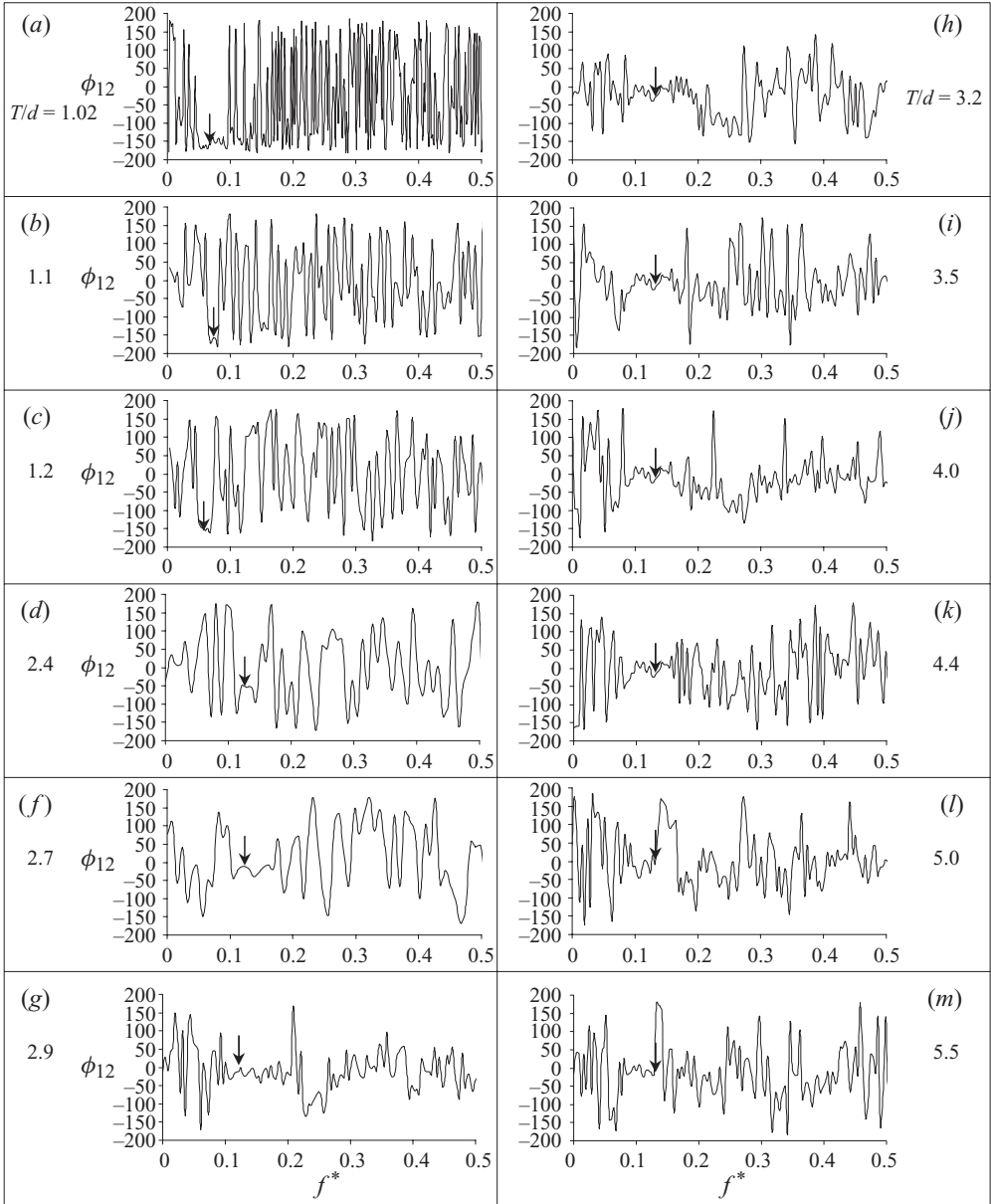
FIGURE 13. Spectral phase ϕ_{12} between u_1 and u_2, captured simultaneously from the two hot wires. The arrow denotes the f^* value at which the co-spectrum or spectral coherence peak occurs (figures 11 and 12).

two cylinders were predominantly anti-phased at $T/d = 2.1$–3.5 but both anti-phased and in-phased at $T/d > 3.5$. Wang & Zhou (2009) observed also in a two side-by-side circular cylinder wake of $Re = 450$ both anti- and in-phased vortex sheddings at $T/d = 3.0$.

It is interesting to quantify the dependence of the flow modes on T/d in regimes C and D. In order to identify the instantaneous anti- and in-phased modes, we define a
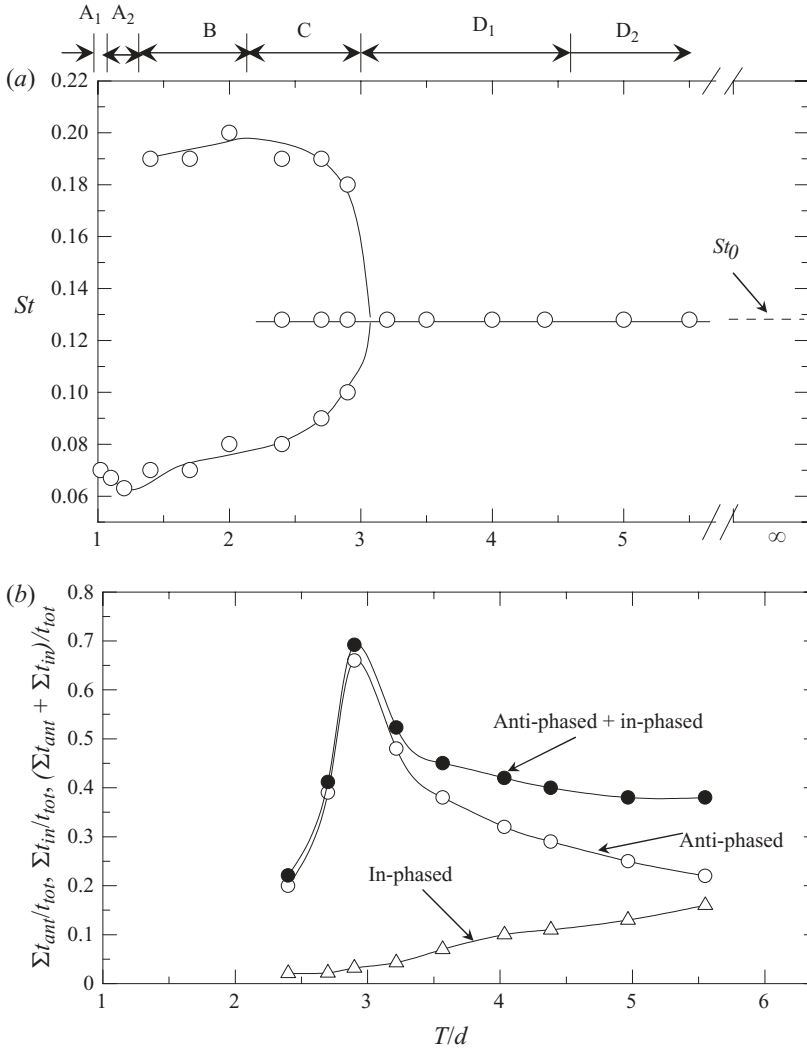
FIGURE 14. (*a*) Dependence of the Strouhal number *St* on *T/d*. The dashed line denotes a single isolated cylinder. (*b*) Comparison in duration between anti- and in-phased vortex sheddings.

local cross-correlation function $R_{u_1 u_2}$ of u_1 and u_2, namely

$$R_{u_1 u_2}(t_i, \tau) = \frac{\displaystyle\sum_{i=t_i-N/2}^{t_i+N/2} \{u_1(i) - \bar{u}_1\}\{u_2(i+\tau) - \bar{u}_2\}}{\sqrt{\displaystyle\sum_{i=t_i-N/2}^{t_i+N/2} \{u_1(i) - \bar{u}_1\}^2 \sum_{i=t_i-N/2}^{t_i+N/2} \{u_2(i+\tau) - \bar{u}_2\}^2}}, \tag{5.1}$$

where t_i is time about which $R_{u_1 u_2}$ is calculated; τ is a time delay or phase shift; $N = 300$ is the number of running points (one vortex shedding period corresponding to about 18 points); and $\bar{u}_1$ and $\bar{u}_2$ are, respectively, the local means of u_1 and u_2, averaged out of the 300 data. At each t_i, the τ_{max} where the maximum magnitude

of $R_{u_1 u_2}$ occurs can be determined, which may nestle between $-180°$ and $180°$. The flow mode is identified to be anti-phased if τ_{max} occurs in the range of $0° \pm 20°$ and in-phased if in the range of $180° \pm 20°$, and the corresponding t_i is denoted by t_{ant} and t_{in}, respectively. The summations of t_{ant} and t_{in} in $t_{tot} \approx 3900$ vortex shedding cycles were obtained and are presented as fractions, i.e. $\Sigma t_{ant}/t_{tot}$ and $\Sigma t_{in}/t_{tot}$, in figure 14(*b*). The remainder $1 - \Sigma t_{ant}/t_{tot} - \Sigma t_{in}/t_{tot}$ is the fraction corresponding to neither anti- nor in-phased flow mode based on the present criteria. In regime C, $\Sigma t_{ant}/t_{tot}$ increases from 20 % at $T/d = 2.4$ to a maximum of 66 % at $T/d = 2.9$. In contrast, $\Sigma t_{in}/t_{tot}$ does not exceed 2 %; that is, the anti-phased mode is predominant. In regime D, $\Sigma t_{ant}/t_{tot}$ decreases and $\Sigma t_{in}/t_{tot}$ increases, reaching about 22 % and 16 %, respectively, at $T/d = 5.5$; their sum drops from about 70 % at $T/d = 3.0$ to 38 % at $T/d = 5.5$. The observation suggests that coupling between the two streets is weakened, as expected, with increasing T/d. Interestingly, whilst the vortices in the anti-phased mode are rapidly reduced, those in the in-phased mode grow.

6. Forces on the cylinders

6.1. *Time history of drag*

Figure 15 illustrates typical instantaneous signals, for a duration of 10 s, of the drag force on a cylinder in different regimes. In sub-regime A_1, where the gap flow is hardly discernible, the signal appears stationary (figure 15*a*). However, the signal in sub-regime A_2 (figure 15*b*) displays abrupt jump and plunge, which is connected to the switch of the gap flow from one side to the other. The narrow street corresponds to higher mean and fluctuating drags than the wide street (figure 15*b*). A similar observation is made in regime B (figure 15*c*). The difference in the magnitude of the drag force before and after the sudden jump is nevertheless smaller than in sub-regime A_2. The signal in regime C is quite different from that in regime A or B. Three modes, i.e. the narrow street, the CVS mode and the wide street, occur. The CVS mode is associated with larger mean and fluctuating drags. On the other hand, the wide-street mode corresponds to the lowest mean and fluctuating drags. The drag signal resumes being stationary in regime D (figure 15*e*).

6.2. *Time-averaged drag and lift*

Since multiple flow modes may occur in regimes A_2, B and C, and their switch appears rather random, the force signals may jump suddenly and are non-stationary. However, the signals may be considered to be stationary within each mode; that is, we may determine the averaged and fluctuating force coefficients for individual modes. A conditional sampling technique was employed for this task. As one example, consider the signal presented in figure 15(*b*), where one section of it is of small magnitude (the wide street) and the other of large magnitude (the narrow street). Local averages, calculated on the basis of the two sections of signal with distinct magnitudes, respectively, yield C_D for the two flow modes. In fact, the probability density function of the signal displays two peaks, each corresponding to C_D for one flow mode. Other force coefficients for individual flow modes are calculated similarly. See Alam *et al.* (2003*a*) for more details of this technique.

To facilitate discussion, assign cylinders 1 and 2 to be associated with the narrow and wide streets, respectively (figure 1). Figure 16(*a*) presents C_D associated with individual cylinders or flow modes and the total time-averaged drag $C_{D,total} = C_{D,cyl.1} + C_{D,cyl.2}$ on the two cylinders, where the subscripts *cyl*.1 and *cyl*.2 refer to cylinders 1 and 2,
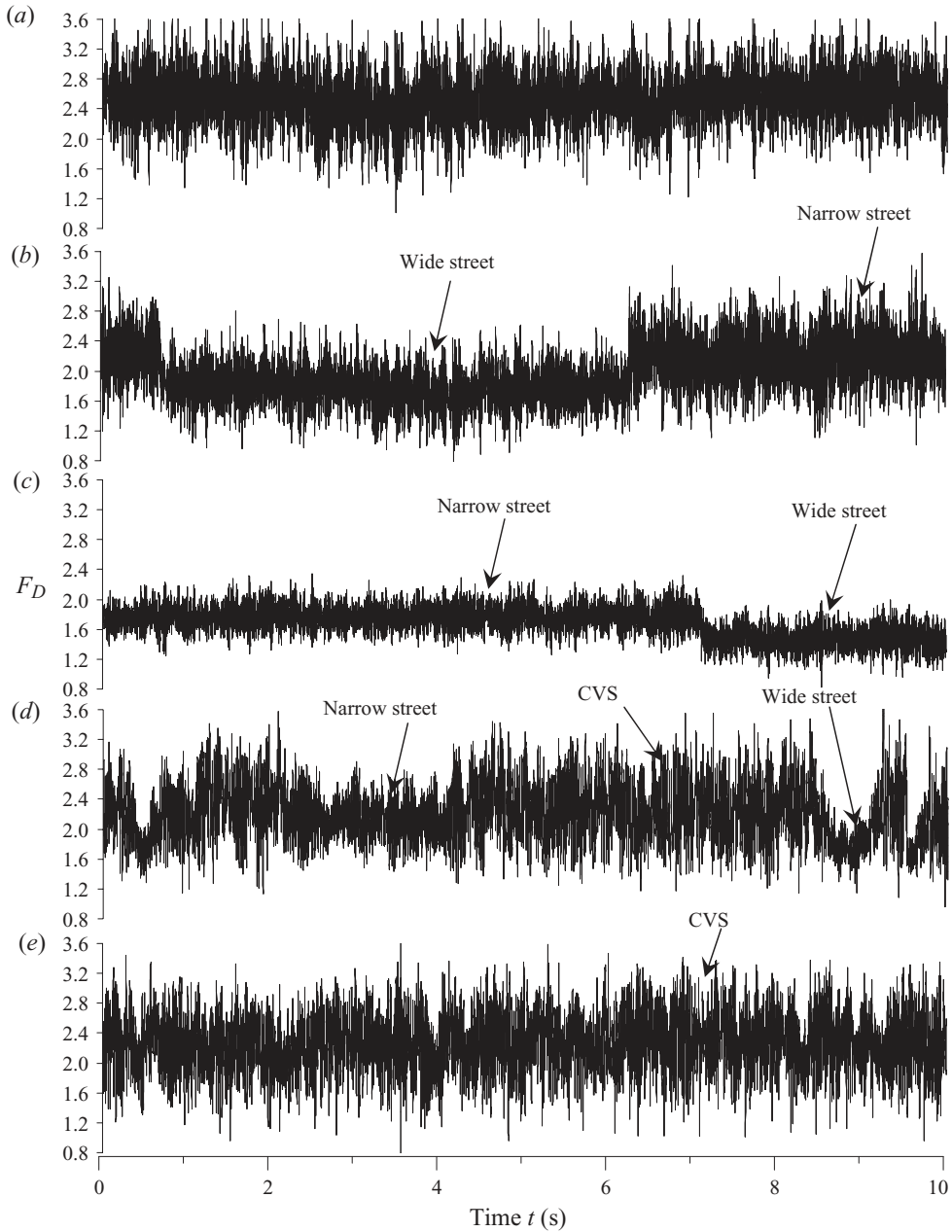
FIGURE 15. Typical instantaneous signals of drag force F_D on cylinder 1: (a) regime A_1 ($T/d = 1.02$), (b) regime A_2 ($T/d = 1.1$), (c) regime B ($T/d = 1.4$), (d) regime C ($T/d = 2.7$) and (e) regime D_1 ($T/d = 3.5$).

respectively. At $T/d = 1.02$ (sub-regime A_1), C_D on one cylinder is the same, 2.54, as on the other, which is about 19 % higher than C_{D0} (= 2.15). At this small T/d, the two cylinders behave like a single rectangular cylinder with $W/H \approx 0.5$, since the gap flow is negligibly small. One question naturally arises: why does each of the two cylinders experience a significantly higher drag than C_{D0}? On a rectangular cylinder,
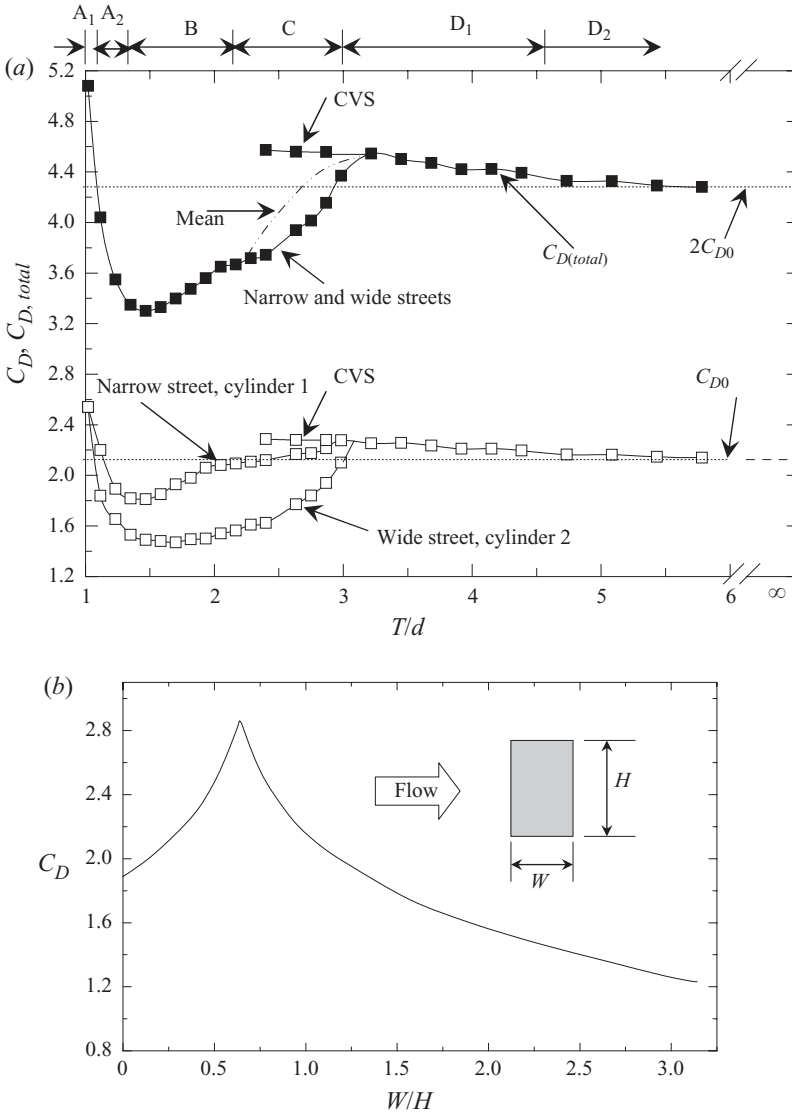
FIGURE 16. (*a*) Dependence on T/d of the time-averaged drag coefficient C_D of individual cylinders (□) and of the total time-averaged drag coefficient $C_{D,total}$ (■). The dashed line denotes a single isolated cylinder, (*b*) Dependence of C_D on W/H of a rectangular cylinder (Courchesne & Laneville 1982); $Re = 6 \times 10^4$ and turbulent intensity $= 0.6\%$.

C_D is highly dependent on W/H. With W/H decreasing from 1.0, C_D rises, reaching its maximum at the critical $W/H = 0.6$ (Bearman & Trueman 1972; Laneville *et al.* 1975; Courchesne & Laneville 1982; Ohya 1994) and then retreats (figure 16*b*). Notably, the C_D values at $W/H = 0.6$ and 0.5 exceeds that at $W/H = 1.0$ by 30 % and 17 %, respectively. Note that the critical W/H may reduce with increasing turbulent intensity (Courchesne & Laneville 1982). The present $C_D = 2.54$ at $T/d = 1.02$ agrees well with previous reports of C_D on a rectangular cylinder with $W/H = 0.5$: 2.75 by Nakamura & Tomonari (1976), 2.5 by Courchesne & Laneville (1982), 2.45 by Bearman & Trueman (1972) and 2.4 by Knisely (1990). This agreement corroborates

our earlier assertion that the effect of the gap flow on the wake can be neglected. It may be concluded that the large C_D at $T/d = 1.02$ results from the effective W/H of near 0.5. As T/d increases from 1.02 to 1.3 (sub-regime A_2), where the two cylinders behave like a single bluff body in terms of St and the effective W/H drops from 0.5 to 0.434, C_D declines rapidly. Two factors are responsible for the observation. Firstly, the gap flow now behaves like a base bleed (Igarashi 1978; Franssona, Koniecznyb & Alfredsson 2004), providing additional streamwise momentum in the near wake and increasing L_f^* and decreasing the magnitude of the base pressure. Secondly, the effective W/H deviates further from 0.5.

In regime B, C_D is small. Note that two cylinders experience different C_D at $T/d = 1.1$–3.0. This difference is greatest at $T/d \approx 2.0$ in regime B. Intuitively, the wider the wake, the higher the value of C_D. In the two side-by-side cylinder wake, however, C_D is smaller in the wide street than in the narrow. The higher C_D associated with the narrow street is mainly due to a short L_f^* (figures 4d and 7) and high wake velocities contributed mostly from the gap flow (figure 5d). As noted by Roshko (1954), 'Generally, for a given cylinder a decrease in wake width corresponds to an increase in drag, which seems at variance with intuition. However, the decrease in width is associated with an increase in "wake velocities", the net effect being an increased wake energy corresponding to the increased drag'.

The three distinct branches of C_D in regime C correspond to the wide, narrow and CVS modes, respectively. The CVS mode has the highest C_D of all, even exceeding C_{D0} because of its shortest L_f^* (figure 7b) and highly coherent vortex shedding (figure 4e_2). In regime D, C_D retreats slowly with increasing T/d, approaching C_{D0} at $T/d \approx 6$.

Sakamoto & Haniu (1988) investigated C_D on two side-by-side square prisms, with an aspect ratio of 3, immersed in a thick turbulent boundary layer at $Re = 1.52 \times 10^5$. Without observing bistable flow, they measured C_D only on one cylinder; C_D tapered from 1.08 to 1.01 with T/d increasing from 1.1 to 1.6, but increased from $T/d = 1.6$ onwards, reaching at $T/d = 6$ the single-cylinder value 1.12, which is about half of the present value (2.15) because their cylinder was immersed in a boundary layer. This variation in C_D is qualitatively similar to the present observation for the wide-street mode. Furthermore, $C_{D,total}$ decreases as T/d increases from 1.02, and reaches the minimum at $T/d = 1.5$, about 24 % lower than C_{D0}. With further increasing T/d, $C_{D,total}$ rises rather rapidly, achieving the maximum at $T/d = 3.2$. The flow mode and $C_{D,total}$ are closely related. In regimes A_2, B and C, $C_{D,total}$ is smaller than $2C_{D0}$ or that in the CVS mode. This is because, as the gap flow turns aside, the whole wake in the biased mode loses streamwise momentum more than that in the CVS mode or the isolated cylinder wake. The variation in $C_{D,total}$ (mean) with T/d in regimes C and D is correlated to the occurrence of the anti-phased flow mode; $C_{D,total}$ (mean) increases in regime C, where the anti-phased mode becomes increasingly predominant for larger T/d (figure 14b). On the other hand, $C_{D,total}$ dwindles as the anti-phased mode occurs less frequently with increasing T/d in regime D.

Figure 17 presents the dependence on T/d of C_L on each of the two cylinders and their sum $C_{L,total}$. For $1.2 \leqslant T/d < 6$, cylinders 1 (lower cylinder, narrow street) and 2 (upper cylinder, wide street; figure 1) experience a positive and a negative C_L (attractive forces), respectively, except at $T/d = 1.9$–2.3, where the wide street also yields a positive C_L. At $T/d = 1.02$, C_L on the upper cylinder is 0.73 and that on the lower cylinder is -0.73 (repulsive forces), implying that the pressure on the outer side surfaces of the two cylinders is less than that on the inner side surfaces. Consider a closed curve enclosing, through the gap, the upper cylinder (figure 4b). The net circulation around the cylinder should be clockwise, as the fluid in the
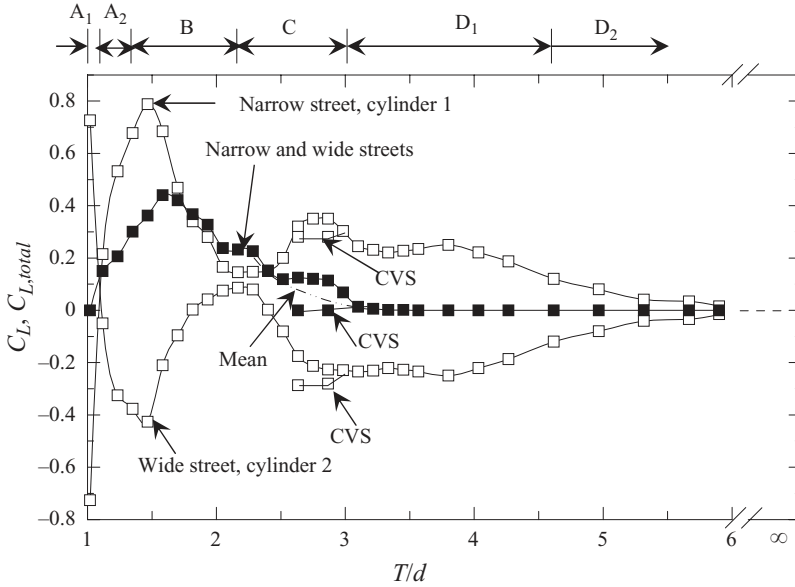
FIGURE 17. Dependence on T/d of the time-averaged lift coefficient C_L of individual cylinders ($\square$) and of the total time-averaged lift coefficient $\bar{C}_{L,total}$ ($\blacksquare$). The dashed line denotes a single isolated cylinder.

gap is virtually stagnant. The clockwise circulation would result in an upward lift (positive). Similarly, the circulation around the lower cylinder should be anticlockwise, producing a negative lift. Since the mean flow about the wake centreline is symmetric (figures 5*b*, 6*b*, 8*b* and 9*b*), the C_L magnitudes of the two cylinders are the same. As T/d increases, the gap flow is jet-like and causes a highly negative pressure on the inner side surfaces, changing the C_L sign of both cylinders and inducing a negative C_L for the upper cylinder (cylinder 2) and a positive C_L for the lower cylinder (cylinder 1). It seems plausible that the gap flow at $T/d = 1.5$ is a highly effective jet, yielding the maximum magnitudes of both negative and positive C_L for cylinders 2 and 1 (figure 17), respectively, and the minimum $C_{D,total}$ (figure 16). As T/d increases from 1.5 to 2.2, the magnitude of C_L drops, since flow between the cylinders approaches that at $T/d = \infty$. Note that at $T/d = 1.1$–2.2 (regimes A_2 and B) the magnitude of positive C_L on cylinder 1 is larger than the negative C_L on cylinder 2. This could be explained in terms of circulation around each cylinder. Since the fluid flows through the gap like a jet, there should be a greater circulation, along the line through the gap, than that along the outer side surfaces. Thus, the net circulation for cylinders 2 and 1 would respectively be anticlockwise and clockwise, yielding negative and positive C_L. On the other hand, the gap flow, deflected towards cylinder 1, contributes more to circulation on the lower cylinder than on the upper, resulting in a larger C_L magnitude on cylinder 1 than that on cylinder 2. The observation is internally consistent with that made earlier from the lateral momentum or $\bar{V}^*$ contours (figure 8) in the near wake ($x^* < 4$), where the negative $\bar{V}^*$-contours behind cylinder 1 overwhelm the positive ones behind cylinder 2.

There is an increase in the C_L magnitude from $T/d = 2.2$ to $T/d = 2.7$, which is ascribed to enhanced anti-phased vortex shedding from the cylinders, as discussed in §§ 3 and 5. Anti-phased vortex shedding prevails at $T/d = 2.7$–4, and the C_L magnitude is in the range of 0.25–03. The predominance of anti-phased and highly
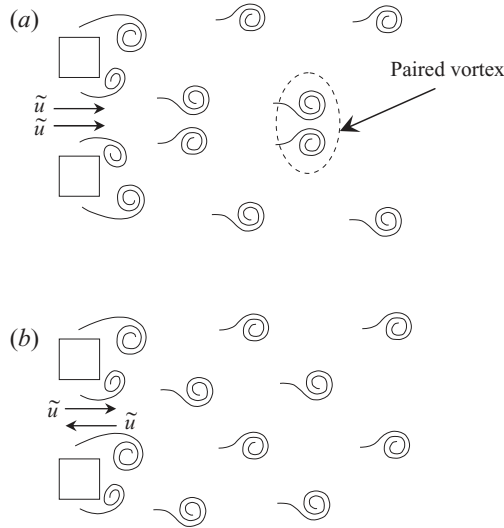
FIGURE 18. (*a*) Anti-phased shedding results in pairing gap vortices; (*b*) in-phased shedding does not. The arrows indicate the direction of fluid motion associated with the gap vortices.

coherent vortex shedding from the two cylinders (figures 11 and 12) is also responsible for the attractive forces between the cylinders. As exemplified in figure 18, the two simultaneously separated opposite-signed gap vortices (figure 18*a*) are close to each other and tend to be paired. This increases significantly the flow velocity about the centreline (Couder & Basdevant 1986; Alam *et al.* 2005) and contributes to a larger circulation through the gap, causing negative and positive C_L (attractive) on cylinders 2 and 1, respectively. A similar observation was made in the wake of two staggered circular cylinders by Alam *et al.* (2005). The attractive forces occurred between the two circular cylinders staggered by an angle of $25°$ at $T/d = 3.1$–5.0 when the vortices separated from the inner side of the two cylinders were paired. From $T/d = 4.0$ to $T/d = 6.0$, the C_L magnitude decreases (figure 17) because intermittently in-phased vortex shedding (figure 18*b*) tends to occur more frequently (figure 14*b*), and the two streets are less coherent (figure 12). Note that, in in-phased shedding, the two oppositely signed gap vortices are shed alternately with a phase angle of $180°$, and their associated motions, $\tilde{u}$, are opposite in phase to each other, as indicated by the arrows in figure 18(*b*). This amounts to adding extra viscous force. On the other hand, both gap vortices separate simultaneously in anti-phased shedding (figure 18*a*), yielding less additional viscous force in the gap flow. The proposition is corroborated by the v^*_{rms}-contours (figure 9g_1,g_2), where v^*_{rms} around the gap centreline ($y^* = 0$) is significantly higher in in-phased than in anti-phased shedding. Therefore, anti-phased vortex shedding induces attractive C_L on the two cylinders. An increase in lateral spacing between the gap vortices also partially contributes to the decreasing C_L magnitude from $T/d = 4.0$ to $T/d = 6.0$ (figure 4*f*,*g*). For finite-length square cylinders submerged in a boundary layer, Sakamoto & Haniu (1988) observed attractive lift forces for the whole range of T/d investigated, with a maximum of 0.22 at $T/d = 1.6$. The C_L magnitude increased from $T/d = 1.1$ to $T/d = 1.6$ and then decreased slowly to C_{L0} at $T/d = 7$.

The combined lift force, i.e. $C_{L,total}$ ($= C_{L,cyl.1} + C_{L,cyl.2}$), is positive at $T/d = 1.1$–3.0, with a maximum $C_{L,total}$ of 0.44 at $T/d = 1.6$. The non-zero $C_{L,total}$ is attributed to

the presence of the biased gap flow. The CVS mode is predominant in regime D, yielding $C_{L,cyl.1} = -C_{L,cyl.2}$ or $C_{L,total} \approx 0$, since the flow structure around one cylinder is similar to the other in both anti- and in-phased arrangements (figures 4–6 and 8). In regimes C and B, the biased flow mode may occur, where the gap flow is deflected from the wide- to the narrow-street cylinder, producing a non-zero $C_{L,total}$. The magnitude of $C_{L,total}$ should be correlated with both the duration of the biased flow mode, compared with other modes, and the extent to which the gap flow is deflected. Note that the gap flow, albeit very small, is biased in regime A_2, resulting in appreciable $C_{L,total}$. At $T/d = 1.02$, $C_{L,total}$ is again zero, though connected to flow physics different from that in regime D; the two cylinders act as a perfect single body. This may be predicted from the time-averaged flow, which is symmetric about the wake centreline (figures 5b, 6b, 8b and 9b); that is, the net circulation enclosing the two cylinders is zero. This provides a rationale to divide regime A into A_1 and A_2.

It is worth pointing out that the combined lift force produced by two cylinders in the biased flow regime may find applications in engineering. For example, a rotating mast of large diameter driven with additional power was previously mounted on a ship for the generation of a lift, as a result of the magnus effect, in a natural wind (Shames 2003). The same function could be performed by two masts placed on or beneath a boat/ship, which may cause the boat/ship to move laterally in a natural wind or water current without any additional consumption of fuel.

6.3. *Fluctuating fluid forces*

The C'_D and C'_L distributions are presented in figure 19. At $T/d = 1.02$, C'_D is 0.69, about 2.37 times larger than C'_{D0}. This large C'_D is not unexpected. With a negligibly small gap flow, the two cylinders behave like a single bluff body, and the effective normalized vortex formation length ($= L_f/2.02d$) is 1.18, much smaller than its single-cylinder counterpart, 1.96 (figure 7). Alternatively, consider the two cylinders to form a rectangular cylinder; this T/d corresponds to a W/H near the critical value at which vortices separated from the outer sides of the two cylinders are greatly strengthened (Bearman & Trueman 1972) and are highly coherent (figure 12). Furthermore, C'_D is measured for only half (one cylinder) of the total body (two cylinders). The large C'_D implies that the in-line flow-induced vibrations of the two square cylinders at $T/d = 1.02$ will be anti-phased and are expected to be very strong.

In the regimes ($T/d = 1.1$–3.0, regimes A_2, B and C) where the gap flow is biased, the narrow street corresponds to a higher C'_D and C'_L than the wide street. Moreover, C'_D and C'_L on both cylinders are small at $1.3 < T/d < 2.2$ (regime B), resulting from weak vortex shedding from the cylinders (figures 4d, 6d, 9d and 12); the difference in C'_D or C'_L between the two cylinders is rather small, with a maximum of 0.01 for C'_D and 0.06 for C'_L. As T/d increases from 2.2 to 2.7, C'_L grows sharply, and the difference in C'_L between the two cylinders is significant, reaching a maximum of 0.45 at $T/d = 2.5$, because of a rapid retreat in L^*_f for the wide street (figure 7). The coherence between vortex sheddings from the two cylinders is also greatly enhanced (figure 12). In regime C, the CVS mode corresponds expectedly to larger C'_D or C'_L than the narrow- or wide-street mode. From $T/d = 3.0$ to $T/d = 5.5$ the coherence between the two streets in the CVS mode is weakened (figure 12). Naturally, both C'_D and C'_L decline. The magnitude of C'_L on both cylinders is large at $T/d = 2.7$–4.6, which is ascribed to the highly coherent anti-phased vortex shedding from the two cylinders (figures 12 and 14b).
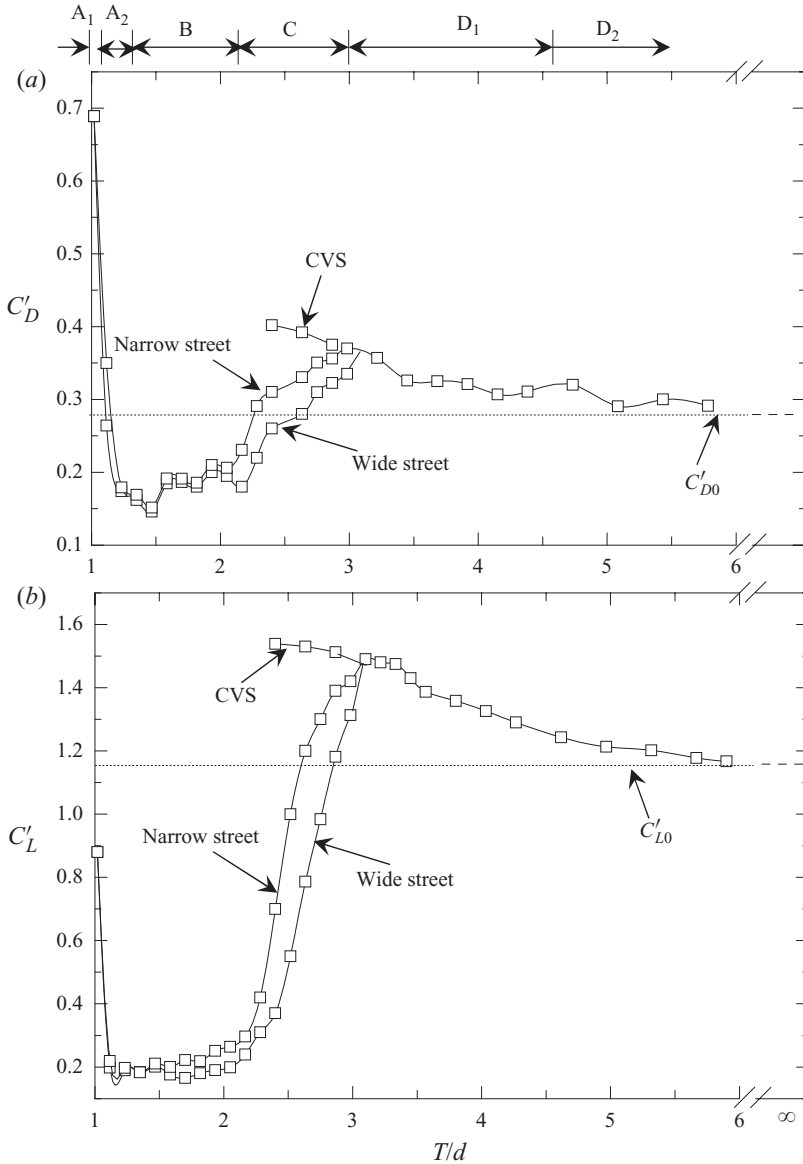
FIGURE 19. Dependence on T/d of (a) the fluctuating drag coefficient C'_D and (b) the fluctuating lift coefficient C'_L. The dashed line denotes a single isolated cylinder.

7. Discussion: flow separation and gap flow passage effects

As discussed in the Introduction, the difference between the square cylinder wake and the circular cylinder wake is in essence the manner in which the flow separates from the cylinders, one with a fixed separation point and the other with a non-stationary oscillating separation point. In the context of two side-by-side cylinders, one additional difference deserves attention, i.e. the passage of the gap flow, in view of the role the gap flow could play in the near-wake dynamics (e.g. Xu *et al.* 2003; Alam & Zhou 2007*a*; Wang & Zhou 2009; Chern *et al.* 2010): one with an unchanged cross-section and the other with a converging and diverging geometry. A comparison

between the observations from the two wakes is insightful for the two effects on the wake dynamics.

Flow classification for the two side-by-side square cylinder wake bears to a degree resemblance to its counterpart of circular cylinders. However, their T/d ranges of different regimes are not quite the same. The bistable gap flow may occur over $T/d = 1.1$–3.0 for the former, but only 1.1–2.5 for the latter (Bearman & Wadcock 1973; Kamemoto 1976; Kim & Durbin 1988; Alam *et al.* 2003*a*; Xu *et al.* 2003). Three flow regimes have been identified for circular cylinders: the single-body regime ($T/d < 1.2$–1.3), the two-frequency regime (1.2–$1.3 < T/d < 2.2$–2.5) and the CVS regime ($T/d > 2.2$–2.5) (e.g. Bearman & Wadcock 1973; Kamemoto 1976; Kim & Durbin 1988). The exact T/d ranges may depend on Re (Xu *et al.* 2003). The single-body regime does not differ much in terms of the T/d range from its counterpart of square cylinders. This is however not the case for other regimes. To our knowledge, the transition regime has never been proposed for the wake of two side-by-side circular cylinders. Nonetheless, Alam *et al.* (2003*a*) did observe three distinct frequencies at $T/d = 1.2$–2.2 in the wake of two side-by-side circular cylinders ($Re = 5.5 \times 10^4$). This T/d range, presumably corresponding to the transition regime of the flow, deviates from that ($T/d = 2.2$–3.0) of the square cylinder case. Furthermore, the CVS regime starts to occur at $T/d = 2.2$, substantially smaller than that ($T/d = 3.0$) for square cylinders. The deviation originates from the fact that the flow separation angle, i.e. the angle between the streamline (or the shear layer) at the separation point and the free-stream flow direction, is larger for the square cylinder than for the circular one (e.g. Hu, Zhou & Dalton 2006). This implies that, given the same T/d, the two inner shear layers and hence the two streets interact more strongly in the case of square cylinders. This result may also be considered from a different perspective. The gap flow goes through a converging and diverging passage for circular cylinders but a constant opening for square cylinders. The latter should be associated with more pressure loss; that is, given the same Re and T/d, the streamwise momentum of flow through the gap of two circular cylinders will be larger than through that of square cylinders. The gap flow of higher streamwise momentum is less prone to be biased (Zhou *et al.* 2009); that is, the biased flow mode starts to recede or cease to occur at a smaller T/d for circular cylinders. This difference is naturally reflected in the measured fluid forces. Moreover, C_D and C_L on two side-by-side circular cylinders (figure 20) are reproduced from Alam *et al.* (2003*a*), whose $Re = 5.5 \times 10^4$ is close to the present 4.7×10^4. The T/d range over which C_D differs considerably in magnitude between the cylinders is 1.1–2.5 for circular cylinders (figure 20) but 1.1–3.0 for square cylinders (figure 16). A similar observation is made in C_L.

The dependence of $C_{D,total}$ on T/d is qualitatively the same (figures 16 and 20*a*) for the two types of cylinders. Both display the minimum $C_{D,total}$ at $T/d = 1.5$, about 24 % and 16 % below their own counterpart $2C_{D0}$, respectively. Note that there is a range of T/d in the biased flow mode for both types of cylinders ($T/d = 1.3$–2.8 for square cylinders and 1.4–1.7 for circular cylinders), where C_D on each of the two bodies dives below C_{D0}. The one corresponding to the wide street is as low as 32 % below C_{D0} for square cylinders at $T/d = 1.7$ and 25 % below C_{D0} for circular cylinders at $T/d = 1.5$. This could be true for any cross-section shape of cylinders or bodies and may find applications. For instance, in horse racing, two side-by-side horses of appropriate spacing may be subjected to less drag than when isolated; the one slightly falling behind produces a wide street, as may be inferred from Hu & Zhou (2008), with its drag being smaller of the two.
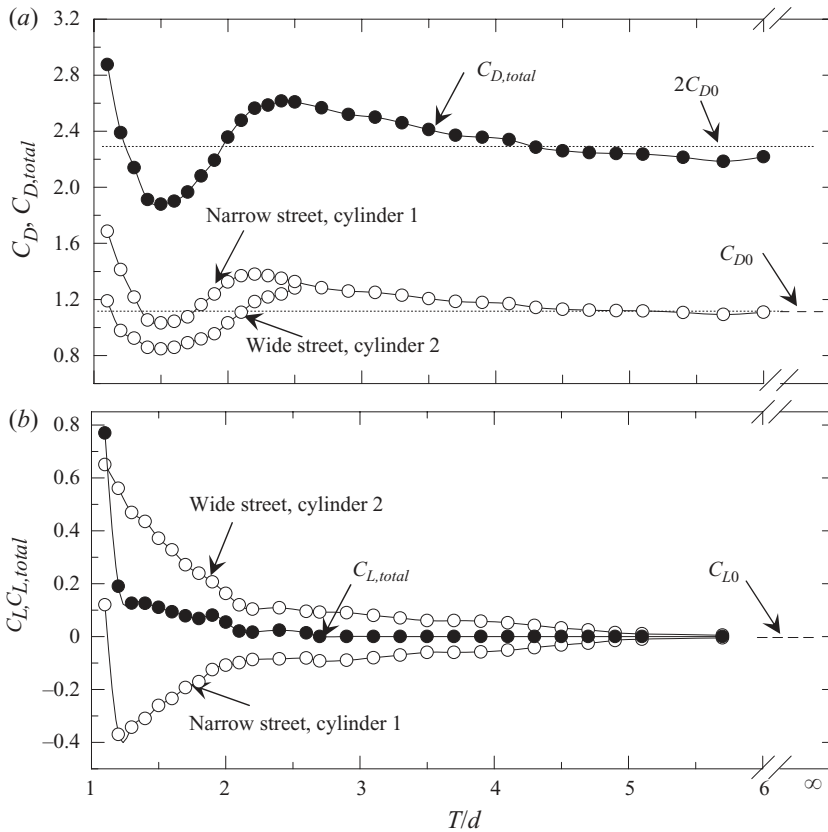
FIGURE 20. For circular cylinder cases: (*a*) the time-averaged drag C_D (○) of individual cylinders and their sum $C_{D,total}$ (●); (*b*) the time-averaged lift coefficient C_L (○) of individual cylinders and their sum $C_{L,total}$ (●) (Alam *et al.* 2003*a*). The dashed line denotes a single isolated cylinder.

The variations of C_L with T/d are qualitatively different between the two types of cylinders (figures 17 and 20*b*). At $T/d \geqslant 1.2$, C_L is positive on square cylinder 1 but negative on square cylinder 2 except at $T/d = 1.9$–2.3, implying that the two square cylinders attract each other. The observation for circular cylinders is however opposite; that is, the two circular cylinders repel each other. The repulsive forces between the circular cylinders are generated by (i) a shift in the forward stagnation point θ_{stg} and hence a shift in the positive pressure region over the cylinder surface towards the gap (e.g. Zhou *et al.* 2001; Alam *et al.* 2003*a*) and (ii) a difference in the separation point θ_s between the two shear layers over a cylinder. On the basis of the measured time-averaged pressure distribution, Alam *et al.* (2003*a*) noted in the wake of two side-by-side circular cylinders that θ_s was 60° for the outer shear layer and −110° for the inner shear layer over cylinder 1 at $T/d = 1.5$, and 70° and −90°, respectively, at $T/d = 2.4$; that is, the outer shear layer separates earlier than the inner shear layer. It is well known that in an isolated cylinder wake a postponed separation corresponds to a higher pressure drop. However, in case of two interfering cylinders, the inner shear layer of a cylinder is strongly interfered with by the other cylinder. As a matter of fact, the magnitude of the minimum pressure, or the maximum pressure drop, on the outer sides of two side-by-side cylinders

was slightly higher than on the inner sides (Alam *et al.* 2003*a*), contributing to the repulsive C_L. On the other hand, C_L on a square cylinder depends only on the pressure difference between the upper and lower surfaces, and any shift in θ_{stg} will have no direct effect on C_L. Furthermore, the flow separation point is fixed at the corner, irrespective of T/d, playing no part in the dependence of C_L on T/d. The attractive C_L originates from the jet-like flow through the gap; the magnitude of C_L is however larger on cylinder 1 than on cylinder 2, since the gap flow biased towards cylinder 1 contributes more to clockwise circulation around cylinder 1 than to anticlockwise circulation around cylinder 2. For the circular cylinder case, the biased gap flow also contributes to circulation about cylinder 1, acting to reduce the magnitude of the repulsive C_L. Therefore, the magnitude of C_L on cylinder 1 is lower than on cylinder 2.

At $T/d \leqslant 1.2$, C_L on cylinder 1 changes from the negative sign at $T/d = 1.2$ to the positive at $T/d = 1.1$ for circular cylinders (figure 20*b*). The positive C_L on cylinder 1 was attributed to the formation of a separation bubble on the cylinder by the biased gap flow (Alam *et al.* 2003*a*; Alam & Zhou 2007*a*). For the square cylinder case, both cylinders change the sign of C_L from $T/d = 1.10$ to $T/d = 1.02$, as the gap flow could be considered to be absent at $T/d = 1.02$ but not at beyond $T/d = 1.10$.

The variation in $C_{L,total}$ is qualitatively different between the two types of cylinders in the T/d ranges in which the gap flow is biased. For square cylinders, $C_{L,total}$ grows rapidly from $T/d = 1.1$ to $T/d = 1.6$ and then diminishes from $T/d = 1.6$ to $T/d = 3.0$; for circular cylinders, it plunges from its maximum (0.77) at $T/d = 1.1$ to 0.2 at $T/d = 1.3$ and then diminishes slowly to zero at $T/d \approx 2.0$. The observation is largely connected to the behaviour of the gap flow. As Sumner *et al.* (1999) observed, the gap flow deflection through the circular cylinders becomes less deflected with increasing T/d, its angle with respect to the flow direction decreasing exponentially from $32°$ at $T/d = 1.15$ to $0°$ at $T/d = 4.00$. On the other hand, the square cylinders of small T/d form a slit of unchanged cross-section, and the gap flow could not be deflected. Only with T/d increasing beyond 1.1 does the gap flow attain adequate room to be deflected towards one cylinder, resulting in the augmentation of $C_{L,total}$ and reaching its maximum (0.44) at $T/d = 1.6$, where the gap flow deflection is perhaps greatest. For larger T/d, the gap flow deflection recedes and accordingly $C_{L,total}$ shrinks, as illustrated in figure 4(*b*–*e*₁, *e*₃). Note that $C_{L,total}$ is always positive in the biased flow regime, irrespective of square or circular cylinders; that is, the resultant lift force is always directed from the cylinder generating the narrow street to that generating the wide street.

A few other aspects of flow physics are worthy of attention in future investigations in order to gain a thorough picture of the two-cylinder wake. As in a single-cylinder wake, the Kelvin–Helmholtz instabilities occur in the shear layers separating from the cylinders. The small-scale instabilities give rise to Reynolds stresses, which will have a substantial influence on the entrainment and thereby the nature of flow separation and vortex formation (Wei & Smith 1986). The three-dimensionality of spanwise vortex rolls is another important aspect; the presence of a neighbouring cylinder may alter the three-dimensional features of the rolls. Finally, as is well recognized, the presence of a global instability in the near wake of a single cylinder is responsible for large-scale vortex formation. How this instability would be altered by an interacting neighbouring wake has yet to be clarified. These aspects have received a great deal of attention in an isolated cylinder wake (e.g. Williamson 1996). It is of fundamental interest to understand how they may be altered by a neighbouring cylinder and how they differ from one regime to another in the wake of two side-by-side cylinders.

8. Concluding remarks

The square cylinder is a representative model for bluff bodies with sharp corners of an infinitely large curvature. Naturally, the findings of the square cylinder wake can be of generalized interest. On the other hand, as the circular cylinder represents another category of bluff bodies with continuous and finite curvature, a comparison between the circular cylinder wake and the square cylinder wake may then provide insight into the difference in physical flow aspects between the two categories of bluff bodies. As such, the major conclusions of this work include two parts: (i) the findings of the two side-by-side square cylinder wake and (ii) comparison with its counterpart of circular cylinders.

Four flow regimes, A, B, C and D, have been identified, each characterized by distinct flow structures, wake characteristic parameters, Strouhal numbers and fluid forces.

In regime A or the single-body regime, the shear layers separating alternately from the outer sides of the two cylinders form a single Kärmän vortex street. Regime A is further divided into two, i.e. the perfectly single-body sub-regime A_1 ($T/d \leqslant 1.02$) and the single-body-like sub-regime A_2 ($1.02 < T/d < 1.3$). The gap flow in A_1 plays no role, and the two cylinders act as a single rectangular cylinder in terms of the drag, lift and St. The same magnitudes of C_D, C_L, C'_D and C'_L act on each cylinder. In A_2 the two cylinders behave like a single body only in terms of St, and the presence of a biased gap flow is clearly discernible, though without adequate strength to divide the wake into two streets. The biased gap flow increases the vortex formation length L_f^* and the wake width w^*, compared with A_1, and differentiates C_D, C_L, C'_D and C'_L on the two cylinders.

In regime B or the two-frequency regime, T/d is in the range of 1.3–2.2, and the gap flow between the two cylinders remains biased and grows to an adequate strength to divide the wake into one narrow and one wide street, corresponding to high and low vortex frequencies, respectively. Furthermore, C_D, C'_D, and C'_L are all smaller than their counterparts in an isolated cylinder wake; the resultant lift force is always positive and significant. Fed with most of the gap flow momentum, the narrow street is characterized by a faster velocity recovery, a shorter L_f^* and larger magnitudes of C_D, C_L, C'_D and C'_L than the wide street.

Regime C occurs at $T/d = 2.2$–3.0 and is also referred to as the transition regime, where the two-frequency shedding mode may be changed intermittently to the coupled vortex shedding mode. As a result, three distinct vortex frequencies occur. Whilst the low and high frequencies are associated with the wide and narrow streets, respectively, the intermediate one is the frequency of coupled vortex shedding from the two cylinders and is about the same as St_0. The two coupled vortex streets are predominantly anti-phased, whose occurrence grows with T/d, accounting for 20 % of the total shedding cycles at $T/d = 2.4$ and reaching 66 % at $T/d = 3.0$. In regime C, because of an increased T/d, the flow streamwise momentum through the gap arises and the gap flow becomes less biased, compared with regime B. Consequently, L_f^* and w^* shrink in the wide street and grow in the narrow one. Moreover, C_D, C'_D and C'_L also increase. The coupled vortex shedding mode in this regime corresponds to larger C_D, C'_D and C'_L but a shorter L_f^* than the wide- or narrow-street mode.

In regime D or the coupled vortex-shedding regime, vortices are separated from the two cylinders at the same frequency as St_0 and maintain a constant phase shift. The two streets are predominantly anti-phased at $T/d = 3.0$–4.6 (sub-regime D_1), whose occurrence accounts for 65 % and 28 % of the total vortices shed at $T/d = 3.0$

and 4.6, respectively, or are both anti-phased and in-phased at $T/d = 4.6$–6.0 (sub-regime D_2), where the anti- and in-phased streets account for 28 % and 11 % of vortex shedding at $T/d = 4.6$ and 20 % and 16 % of vortex shedding at $T/d = 5.5$, respectively. In sub-regime D_1, C_D, C_L, C'_D, C'_L, L^*_f and w^* are all slightly higher than their counterparts in sub-regime D_2 or those in an isolated cylinder wake probably because the anti-phased vortex streets are better correlated and more persistent (e.g. Zhou *et al.* 2002) than the in-phased streets.

The flow exhibits a number of important differences from that behind circular cylinders, which are all connected to the distinct manners in which the shear layers separate between the flows. (i) The gap flow remains biased over $T/d = 1.1$–3.0 for the square cylinders, larger than that (1.1–2.5) for the circular cylinders. Two factors are responsible. Firstly, the angle of shear layer separation (with respect to free stream) from the cylinder is larger for a square cylinder, resulting in interactions between the two inner shear layers even at a larger T/d. Secondly, the converging and diverging flow passage between two circular cylinders implies a smaller pressure loss than the constant passage between two square cylinders; that is, given the same T/d, the gap flow through the passage between two circular cylinders possesses a larger streamwise momentum than that through the passage between two square cylinders. The gap flow of a larger streamwise momentum is less prone to getting biased. (ii) Although the C_D, C'_D and C'_L distributions are qualitatively the same for the two types of the cylinders, the C_L distributions are not, which is connected to the manner of flow separation from the cylinders and the behaviours of the gap flow. (iii) The lift forces are repulsive for two circular cylinders but attractive for two square cylinders at $T/d \geqslant 1.2$. The attractive forces on the square cylinders originate from the jet-like flow through the gap, which produces a low pressure in the gap. The repulsive forces on the circular cylinders result from a shift in the forward stagnation point towards the gap and early separation of outer shear layer, compared with that of the inner shear layer, which overwhelm that of the jet-like flow through the gap. (iv) The resultant lift force $C_{L,total}$ rises significantly for square cylinders but drops for circular cylinders from $T/d = 1.2$ to $T/d = 1.6$. The observation is ascribed to the fact that, whilst the gap flow through a converging and diverging passage between the circular cylinders is highly deflected at $T/d \approx 1.2$ and becomes less so with increasing T/d, the gap flow through a slit-like passage between the square cylinders, not highly deflected at small T/d, is progressively more deflected.

REFERENCES

ACHENBACH, E. 1968 Distribution of local pressure and skin friction around a circular cylinder in cross-flow up to $Re = 5 \times 10^6$. *J. Fluid Mech.* **34**, 625–639.

AGRAWAL, A., DJENIDI, L. & ANTONIA, R. A. 2006 Investigation of flow around a pair of side-by-side square cylinders using the lattice Boltzmann method. *Comput. Fluids* **35**, 1093–1107.

ALAM, M. M., MORIYA, M. & SAKAMOTO, H. 2003*a* Aerodynamic characteristics of two side-by-side circular cylinders and application of wavelet analysis on the switching phenomenon. *J. Fluids Struct.* **18**, 325–346.

ALAM, M. M., MORIYA, M., TAKAI, K. & SAKAMOTO, H. 2002 Suppression of fluid forces acting on two square cylinders in a tandem arrangement by passive control of flow. *J. Fluids Struct.* **16**, 1073–1092.

ALAM, M. M. & SAKAMOTO H. 2005 Investigation of Strouhal frequencies of two staggered bluff bodies and detection of multistable flow by wavelets. *J. Fluids Struct.* **20** (3), 425–449.

ALAM, M. M., SAKAMOTO, H. & MORIYA, M. 2003*b* Reduction of fluid forces acting on a single circular cylinder and two circular cylinders by using tripping rods. *J. Fluids Struct.* **18**, 347–366.

ALAM, M. M., SAKAMOTO H. & ZHOU, Y. 2005 Determination of flow configurations and fluid forces acting on two staggered circular cylinders of equal diameter in cross-flow. *J. Fluids Struct.* **21**, 363–394.

ALAM, M. M. & ZHOU, Y. 2007*a* Flow around two side-by-side closely spaced circular cylinders. *J. Fluids Struct.* **23** (5), 799–805.

ALAM, M. M. & ZHOU, Y. 2007*b* The turbulent wake of an inclined cylinder with water running. *J. Fluid Mech.* **589**, 261–303.

ALAM, M. M., ZHOU, Y., YANG, H. X., GUO, H. & MI, J. 2010 The ultra-low Reynolds number airfoil wake. *Exp. Fluids* **48**, 81–103.

BALACHANDAR, S., MITTAL, R. & NAJJAR, F. M. 1997 Properties of the mean recirculation region in the wakes of two-dimensional bluff bodies. *J. Fluid Mech.* **351**, 167–199.

BATHAM, J. P. 1973 Pressure distribution on circular cylinders at critical Reynolds numbers. *J. Fluid Mech.* **57**, 209–228.

BEARMAN, P. W. & OBAJASU, E. D. 1982 An experimental study of pressure fluctuations on fixed and oscillating square section cylinders. *J. Fluid Mech.* **119**, 297–321.

BEARMAN, P. W. & TRUEMAN, D. M. 1972 An investigation of the flow around rectangular cylinders. *Aeronaut. Q.* **XXIII** (Pt 3), 229–237.

BEARMAN, P. W. & WADCOCK. A. J. 1973 The interaction between a pair of circular cylinder normal to a stream. *J. Fluid Mech.* **61**, 499–511.

BIERMANN, D. & HERRNSTEIN, W. H. JR 1933 The interference between struts in various combinations. *NACA Tech. Rep.* 468.

BLOOR, S. M. 1964 The transition to turbulence in the wake of a circular cylinder. *J. Fluid Mech.* **19**, 290–309.

CHERN M., KANNA, R., LU, Y., CHENG, I. & CHANG, S. 2010 A CFD study of the interaction of oscillatory flows with a pair of side-by-side cylinders. *J. Fluids Struct.* **26**, 626–643.

COUDER, Y. & BASDEVANT, C. B. 1986 Experimental and numerical study of vortex couples in two-dimensional flows. *J. Fluid Mech.* **173**, 225–251

COURCHESNE, J. & LANEVILLE, A. 1982 An experimental evaluation of drag coefficient for two-dimensional rectangular cylinders exposed to grid turbulence. *ASME J. Fluids Engng* **104**, 523–528.

FARELL, C., CARRASQUEL, S., GUVEN, O. & PATEL, V. C. 1977 Effect of wind tunnel walls on the flow past circular cylinder and cooling tower models. *J. Fluids Engng* **99**, 470–490.

FRANSSONA, J. H. M., KONIECZNYB, P. & ALFREDSSON, P. H. 2004 Flow around a porous cylinder subject to continuous suction or blowing. *J. Fluids Struct.* **198**, 1031–1048.

GERRARD, J. H. 1966 The mechanics of the formation region of vortices behind bluff bodies. *J. Fluid Mech.* **25**, 401–413.

GRIFFIN, O. M. & RAMBERG, S. E. 1974 The vortex street wakes of a vibrating cylinders. *J. Fluid Mech.* **66**, 729–738.

HORI, E. 1959 Experiments on flow around a pair of parallel circular cylinders. In *Proceedings of 9th Japan National Congress for Applied Mechanics*, paper III-11, pp. 231–234.

HU, J. C. & ZHOU, Y. 2008 Flow structure behind two staggered circular cylinders. Part 1. Downstream evolution and classification. *J. Fluid Mech.* **607**, 51–80.

HU, J. C., ZHOU, Y. & DALTON, C. 2006 Effects of the corner radius on the near wake of a square prism. *Exp. Fluids* **40**, 106–118.

HUANG, J. F., ZHOU, Y. & ZHOU, T. M. 2006 Three-dimensional wake structure measurement using a modified PIV technique. *Exp. Fluids* **40**, 884–896.

IGARASHI, T. 1978 Flow characteristics around a circular cylinder with a slot. *Bull. JSME* **21** (154), 656–664.

ISHIGAI, S., NISHIKAWA, E., NISHIMURA, E. & CHO, K. 1972 Experimental study of structure of gas flow in tube banks axes normal to flow. *Bull. Japan Soc. Mech. Eng.* **15**, 949–956.

JENDRZEJCZYK, J. A. & CHEN, S. S. 1982 Fluid forces on two circular cylinders in liquid crossflow. *ASME PVP* **63**, 31–44.

KAMEMOTO, K. 1976 Formation and interaction of two parallel vortex streets. *Bull. Japan Soc. Mech. Eng.* **19**, 283–290.

KIM, H. J. & DURBIN, P. A. 1988 Investigation of the flow between a pair of circular cylinders in the flopping regime. *J. Fluid Mech.* **196**, 431–448.

KIYA, M., ARIE, M., TAMURA, H. & MORI, H. 1980 Vortex shedding from two circular cylinders in staggered arrangement. *ASME J. Fluids Engng* **102**, 166–173.

KNISELY, C. W. 1990 Strouhal numbers of rectangular cylinders at incidence: a review and new data. *J. Fluids Struct.* **4**, 370–393.

KOLÁŘ, V., LYN, D. A. & RODI, W. 1997 Ensemble-averaged measurements in the turbulent near wake of two side-by-side square cylinders. *J. Fluid Mech.* **346**, 201–237.

LANEVILLE, A., GARTSHORE, I. S. & PARKINSON, G. V. 1975 An explanation of some effects of turbulence on bluff bodies. In *Proceedings of the Fourth International Conference Wind Effects on Buildings & Structure, Heathrow, UK , K75–363* (ed. K. J. Eator), pp. 333–341. Cambridge University Press.

LEE, B. E. 1975 The effect of turbulence on the surface pressure field of a square prism. *J. Fluid Mech.* **69**, 263–282.

LESAGE, F. & GARTSHORE, I. S. 1987 A method of reducing drag and fluctuating side force on bluff bodies. *J. Wind Engng Indust. Aerodyn.* **25**, 229–245.

MENEGHINI, J. R., SALTARA, F., SIQUIRA, C. L. R. & FERRARI, J. A. 2001 Numerical simulation of flow interference between two circular cylinders in tandem and side-by-side arrangements. *J. Fluids Struct.* **15**, 327–350.

MORETTI, P. 1993 Flow-induced vibration in arrays of cylinders. *Annu. Rev. Fluid Mech.* **25**, 99–114.

NAKAGAWA, S., NITTA, K. & SENDA, M. 1999 An experimental study on unsteady turbulent near wake of a rectangular cylinder in channel flow. *Exp. Fluids* **27**, 284–294.

NAKAGUCHI, H., HASIMOTO, K. & MUTO, S. 1968 An experimental study of aerodynamic drag on rectangular cylinders. *J. Japan Soc. Aeronaut. Space Sci.* **16**, 1–5.

NAKAMURA, Y. & TOMONARI, Y. 1976 The effect of turbulence on the drag of rectangular prisms. *J. Japan Soc. Aeronaut. Space Sci.* **19** (44), 81–86.

NODA, H. & NAKAYAMA, A. 2003 Free-stream turbulence effects on the instantaneous pressure and forces on cylinders of rectangular cross section. *Exp. Fluids* **34**, 332–344.

NORBERG, C. 1993 Flow around rectangular cylinders: pressure forces and wake frequencies. *J. Wind Engng Indust. Aerodyn.* **49**, 187–196.

NOVAK, J. 1974 Strouhal number of a quadrangular prism, angle iron and two circular cylinders arranged in tandem. *Acta Tech. CSAV* **19** (3), 361–373.

OHYA, Y. 1994 Note on a discontinuous change in wake pattern for a rectangular cylinder. *J. Fluids Struct.* **8**, 325–330.

OKAJIMA, A. 1982 Strouhal number of rectangular cylinders. *J. Fluid Mech.* **123**, 379–398.

OUDHEUSDEN, B. W., SCARANO, F., HINSBERG, N. P .V. & ROOSENBOOM, E. W. M. 2008 Quantitative visualization of the flow around a square-section cylinder at incidence. *J. Wind Engng Indust. Aerodyn.* **96**, 913–922.

PARANTHOEN, P., BROWNE, L. W. B., MASSON, S. L., DUMOUCHEL, F. & LECORDIER, J. C. 1999 Characteristics of the near wake of a cylinder at low Reynolds numbers. *Eur. J. Mech. B/Fluids* **18**, 659–674.

RAMBERG, S. E. 1983 The effects of yaw and finite length upon the vortex wakes of stationary and vibrating circular cylinders. *J. Fluid Mech.* **128**, 81–107.

RAO, Y. NI, Y., & LIU, C. 2008 Flow effect around two square cylinders arranged side-by-side using lattice Boltzmann method. *Intl J. Mod. Phys. C* **19**, 1683–1694.

REINHOLD, T. A., TIELEMAN, H. W. & MAKER, F. J. 1977 Interaction of square prisms in two flow fields. *J. Indust. Aerodyn.* **2**, 223–241.

ROSHKO, A. 1993 Perspectives on bluff body aerodynamics. *J. Wind Engng Indust. Aerodyn.* **49**, 79–100.

ROSHKO, A. 1954 On the drag and shedding frequency of two-dimensional bluff bodies. *NACA Tech. Note* 3169.

SAKAMOTO, H. & HANIU, H. 1988 Effect of free stream turbulence on characteristics of fluctuating forces acting on two square prisms in tandem arrangement. *ASME J. Fluids Engng* **110**, 140–146.

SAKAMOTO, H., HANIU, H. & OBATA, Y. 1987 Fluctuating forces acting on two square prisms in a tandem arrangement. *J. Wind Engng Indust. Aerodyn.* **26**, 85–103.

SAKAMOTO, H. & OIWAKE, S. 1984 Fluctuating forces on a rectangular prism and a circular cylinder placed vertically in a turbulent boundary layer. *ASME J. Fluids Engng* **106**, 160–166.

SHAMES, I. H. 2003 *Mechanics of Fluids*, 4th edn. McGraw-Hill.

SPIVACK, H. M. 1946 Vortex frequency and flow pattern in the wake of two parallel cylinders at varied spacing normal to an air stream. *J. Aeronaut. Sci.* **13**, 289–301.

SUMNER, D., WONG, S. S. T., PRICE, S. J. & PAIDOUSSIS, M. P. 1999 Fluid behavior of side-by-side circular cylinders in steady cross-flow. *J. Fluids Struct.* **13**, 309–339.

SURRY, D. 1972 Some effects of intense turbulent on the aerodynamic of a circular cylinder at subcritical Reynolds number. *J. Fluid Mech.* **52** (Pt 2), 543–563.

SZEPESSY, S. & BEARMAN, P. W. 1992 Aspect ratio and end plate effects on vortex shedding from a circular cylinder. *J. Fluid Mech.* **234**, 191–217.

TAMURA, T. & MIYAGI, T. 1999 The effect of turbulence on aerodynamic forces on a square cylinder with various corner shapes. *J. Wind Engng Indust. Aerodyn.* **83**, 135–145.

THOMAS, O. G. & KRAUS, K. A. 1964 Interaction of vortex streets. *J. Appl. Phys.* **365**, 3458–3459.

VENUGOPAL, V., VARYANI, K. S. & BARLTROP, N. D. P. 2006 Wave force coefficients for horizontally submerged rectangular cylinders. *Ocean Engng* **33**, 1669–1704.

VICKERY, B. J. 1966 Fluctuating lift and drag on a long cylinder of square cross-section in a smooth and in a turbulent stream. *J. Fluid Mech.* **25**, 481–494.

WANG, H. F. & ZHOU, Y. 2009 The finite-length square cylinder near wake. *J. Fluid Mech.* **638**, 453–490.

WANG, Z. J. & ZHOU, Y. 2005 Vortex interaction in a two side-by-side cylinder near-wake. *Intl J. Heat Fluid Flow* **26**, 362–377.

WEI, T. & SMITH, C. R. 1986 Secondary vortices in the wake of circular cylinders. *J. Fluid Mech.* **169**, 513–533.

WEST, G. S. & APELT, C. J. 1982 The effect of tunnel blockage and aspect ratio on mean flow past a circular cylinder with Reynolds number between 10^4 to 10^5. *J. Fluid Mech.* **14**, 361–377.

WEST, G. S. & APELT, C. J. 1993 Measurements of fluctuating pressures and forces on a circular cylinder in the Reynolds number range 10^4 to 2.5×10^5. *J. Fluids Struct.* **7**, 227–244.

WEST, G. S. & APELT, C. J. 1997 Fluctuating lift and drag forces on finite lengths of a circular cylinder in the subcritical Reynolds number range. *J. Fluids Struct.* **11**, 135–158.

WILLIAMSON, C. H. K. 1996 Vortex dynamics in the cylinder wake. *Annu. Rev. Fluid Mech.* **28**, 477–526.

XU, S. J., ZHOU, Y. & SO, R. M. C., 2003 Reynolds number effects on the flow structure behind two side-by-side cylinders. *Phys. Fluids* **15**, 1214–1219.

ZDRAVKOVICH, M. M. 1977 Review of flow interference between two circular cylinders in various arrangements. *ASME J. Fluids Engng* **199**, 618–633.

ZDRAVKOVICH, M. M. & PRIDDEN, D. L. 1977 Interference between two circular cylinders; series of unexpected discontinuities. *J. Indust. Aerodyn.* **2**, 255–270.

ZHOU, Y., FENG, S. X., ALAM, M. M. & BAI, H. L. 2009 Reynolds number effect on the wake of two staggered cylinders. *Phys. Fluids* **21**, 125105, 14pp.

ZHOU, Y., WANG, Z. J., SO, R. M. C., XU, S. J. & JIN, W. 2001 Free vibrations of two side-by-side cylinders in a cross-flow. *J. Fluid Mech.* **443**, 197–229.

ZHOU, Y., ZHANG, H. J. & YIU, M. W. 2002 The turbulent wake of two side-by-side circular cylinders. *J. Fluid Mech.* **458**, 303–332.